

1 **Atmospheric and surface observations during the Saint John**  
2 **River Experiment on Cold Season Storms (SAJESS)**

3 Hadleigh D. Thompson<sup>1</sup>, Julie M. Thériault<sup>1</sup>, Stephen J. Déry<sup>2</sup>, Ronald E. Stewart<sup>3</sup>, Dominique  
4 Boisvert<sup>1</sup>, Lisa Rickard<sup>2</sup>, Nicolas R. Leroux<sup>1</sup>, Matteo Colli<sup>5</sup> and Vincent Vionnet<sup>4</sup>

5  
6 <sup>1</sup>Department of Earth and Atmospheric Sciences, Centre ESCER, Université du Québec à Montréal, Montréal,  
7 Québec, H3C 3P8, Canada

8 <sup>2</sup>Department of Geography, Earth and Environmental Sciences and Natural Resources and Environmental Studies  
9 Program, University of Northern British Columbia, Prince George, British Columbia, V2N 4Z9, Canada

10 <sup>3</sup>Department of Environment and Geography, University of Manitoba, Winnipeg, Manitoba, R3T 2N2, Canada

11 <sup>4</sup>Meteorological Research Division, Environment and Climate Change Canada, Dorval, Quebec, H9P 1J3, Canada

12 <sup>5</sup>Artys Srl, Piazza della Vittoria, 9/3, 16121 Genova, Italy

13 *Correspondence to:* Julie M. Thériault (theriault.julie@uqam.ca)

14 **Running title**

15 Data from the Saint John River Experiment on Cold Season Storms (SAJESS)

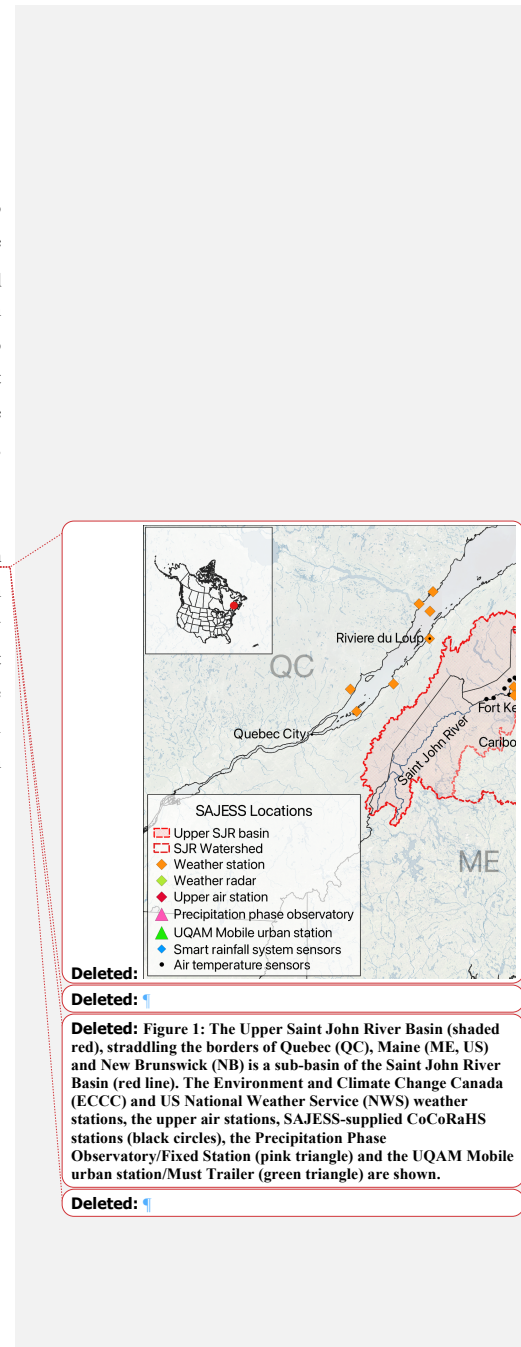
16 **Abstract.** The amount and phase of cold season precipitation accumulating in the upper Saint John River basin,  
17 are critical factors in determining spring runoff, ice-jams, and flooding in downstream communities. To study the  
18 impact of winter and spring storms on the snowpack in the upper Saint John River (SJR) basin. The region  
19 encompasses parts of the US state of Maine (ME) and the Canadian provinces of Quebec (QC) and New  
20 Brunswick (NB). The Saint John River Experiment on Cold Season Storms (SAJESS) utilized meteorological  
21 instrumentation, upper air soundings, human observations, and hydrometeor macrophotography during  
22 winter/spring 2020-21. Here, we provide an overview of the SAJESS study area, field campaign. Firstly,  
23 meteorological instrumentation was co-located with an Environment and Climate Change Canada station near  
24 Edmundston, New Brunswick, in early December 2020. This was followed by an intensive observation period  
25 that included manual observations, upper-air soundings, a multi-angle snowflake camera, macrophotography of  
26 solid hydrometeors throughout March and April 2021. A lower-than-average snowpack peaked at ~65 cm, with a  
27 total of 287 mm of precipitation (liquid equivalent) falling between December 2020 and April 2021, a 21% lower  
28 amount of precipitation than the climatological normal. Observers were present for 13 storms, conducting manual  
29 observations for 183 hours of precipitation, while taking more than 4000 images of hydrometeors. The inclusion  
30 of local volunteers and schools provided an additional 1700 measurements of precipitation amounts. The resulting  
31 datasets include optical disdrometer data, micro rain radar output, near-surface meteorological observations, as  
32 well as temperature, pressure, humidity, and precipitation data. These data are publicly available from the  
33 Federated Research Data Repository at <https://doi.org/10.20383/103.0591> (Thompson et al., 2023). We also  
34 include a synopsis of the data management plan and data processing, and a brief assessment of the rewards and  
35 challenges of utilizing community volunteers for hydro-meteorological citizen science.

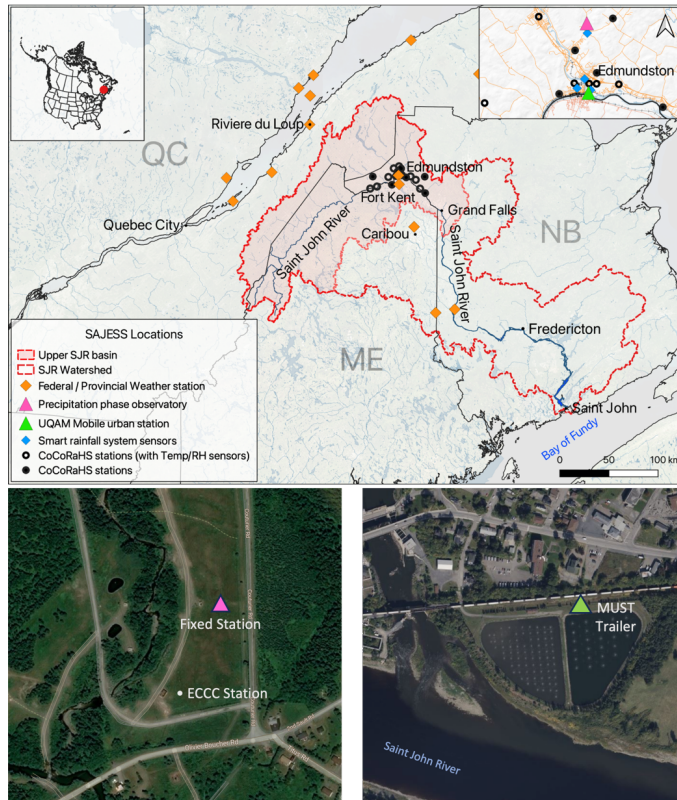
36 **1 Introduction**

37 The Saint John River Experiment on Cold Season Storms (SAJESS) focused on cold region processes related to  
38 winter and spring storms over the transboundary upper Saint John River basin, located on the border of Maine  
39 (ME) and the provinces of Quebec (QC) and New Brunswick (NB). The Saint John River, known as the Wolastoq  
40 by local Indigenous communities, is 673 km long and drops 480 m in elevation from its source at the Little John  
41 River (ME) down to the Bay of Fundy (Fig. 1). **The Saint John River watershed** covers 55,000 km<sup>2</sup>, with 36%  
42 located in the U.S., although, here we define the upper Saint John River basin as the area that drains into the Saint  
43 John River above Grand Falls, NB. Economically important to the region, the river provides flow for five  
44 hydroelectric facilities with development being overseen by the International Joint Commission (Kenny & Secord,  
45 2010).

46  
47 **A concern of emergency managers along the Saint John River is the risk of catastrophic flooding when spring rain**  
48 **coincides with relatively high temperatures, creating significant snow melt.** Such flooding events occurred in  
49 2008, 2018, and again in 2019, and were in the annual top 10 Canadian weather disasters identified by  
50 Environment and Climate Change Canada (ECCC) (ECCC, 2017, 2019, 2020). Although this sub-catchment  
51 covers an area of 22,600 km<sup>2</sup>, **most of** the research focusing on the Saint John River does so by examining the  
52 lower reaches and associated lakes, wetlands, and tidal estuaries. There is therefore a paucity of both hydrological  
53 knowledge of the upper basin, as noted by Budhathoki et al. (2022), and meteorological stations (only two within  
54 the upper SJR basin) (also see Fortin and Dubreuil, 2020).

55





68

69 Figure 1: Top: The Upper Saint John River Basin (shaded red), straddling the borders of Quebec (QC), Maine (ME,  
 70 US) and New Brunswick (NB) is a sub-basin of the Saint John River Basin (red line). The Environment and Climate  
 71 Change Canada (ECCC) and US National Weather Service (NWS) weather stations, SAJESS-supplied CoCoRaHS  
 72 stations including where Temperature/RH sensors were also co-located, (black circles), the Precipitation Phase  
 73 Observatory/Fixed Station (pink triangle) and the UQAM Mobile urban station/MUST Trailer (green triangle) are  
 74 shown. Bottom: Aerial photographs of the two main SAJESS sites showing the locations of the Fixed Station, MUST  
 75 Trailer, and ECCC Station. Microsoft product screenshots reprinted with permission from Microsoft Corporation.

76



77 There have been several previous cold-season precipitation studies in North America. These include a comparison  
78 between orographic winter storms in the San Juan Mountains and Sierra Nevada by Marwitz (1986), the Canadian  
79 Atlantic Storms Program (Stewart et al., 1987; Stewart, 1991) that investigated the synoptic and mesoscale  
80 structure of Canadian East Coast winter storms, and field campaigns such as the meteorological monitoring  
81 network established for the Vancouver 2010 winter Olympics (Joe et al., 2014), and the Olympic Mountains  
82 experiment (OLYMPEX) that studied the modification of Pacific storms by coastal mountain ranges (Houze et  
83 al., 2017). Notably, the Vancouver Olympics network utilized a first-generation hotplate precipitation gauge, and  
84 while OLYMPEX used similar instrumentation to SAJESS such as disdrometers, weighing rain gauges, and micro  
85 rain radars, they also employed instrumented aircraft and a greater range of radar options. Ongoing research into  
86 East Coast snowstorm-producing cyclones is being undertaken by the Investigation of Microphysics and  
87 Precipitation for Atlantic Coast-Threatening Snowstorms (IMPACTS) campaign. Similar to OLYMPEX,  
88 IMPACTS combines surface observations and measurements with airborne remote sensing instruments. In terms  
89 of field projects, SAJESS compares closest to the recent (2019) Storms and Precipitation Across the continental  
90 Divide experiment (SPADE) (Thériault et al., 2021a, 2022), adopting the methods of manual observations,  
91 macrophotography, and micro rain radar and disdrometer deployment, although we built on SPADE by adding a  
92 distributed network of temperature and precipitation measurements, and upper air observations.

93  
94 Locally, previous studies encompassing the Saint John River Basin have focused on flooding (Newton & Burrell,  
95 2016), including rain-on-snow events (Buttle et al., 2016), and the analysis and modeling of ice jams that may  
96 increase in frequency in future climate scenarios (Beltaos et al., 2003). Despite these hazards, no studies of storms  
97 and precipitation and their impact on snowpack evolution have been conducted in this region.

98  
99 The SAJESS dataset contains meteorological and precipitation data that were collected at a fixed station from 1  
100 December 2020 until 30 April 2021, and an intensive observation period (IOP) that took place from 8 March to  
101 30 April 2021. The objective of this paper is to describe the data collected during SAJESS, provide examples of  
102 the measurements and how they can be combined to broaden the picture of meteorological conditions observed,  
103 and to illustrate to stakeholders and potential users the importance of the field campaign and dataset.

104  
105 The paper is organized as follows: the sites used during SAJESS are described in Section 2; the instruments,  
106 manual observations, and other sources of data are detailed in Section 3; an overview of data processing,

107 [management, and validity, along with examples of data collected throughout SAJESS are presented in Section 4;](#)  
108 [and a summary, including a discussion on potential future analyses, is given in Section 5.](#)

## 109 **2 Site Descriptions**

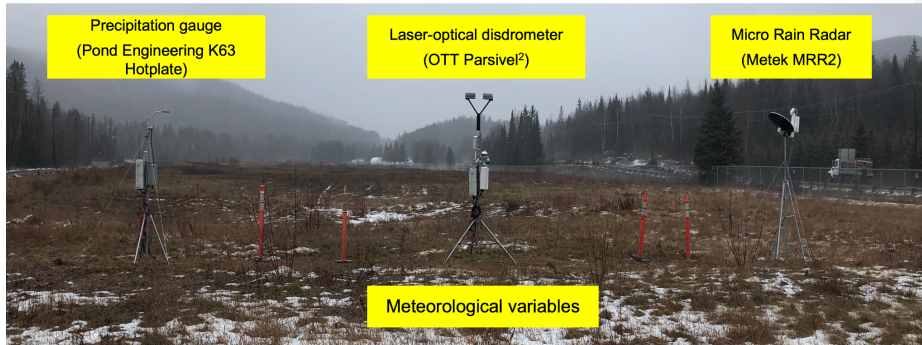
### 110 **2.1 Overview**

111 To observe the spatial and temporal variability in precipitation amount and phase across the study area, a broad  
112 range of techniques was employed: first, a semi-permanent ‘Precipitation Phase Observatory’ was installed to  
113 record meteorological data from December 2020 to April 2021. This site became known as the ‘Fixed Station’  
114 and was co-located with the permanent ECCC station, north of Edmundston (Fig. 1). Second, the Mobile Urban  
115 Station (MUST), a modified enclosed trailer provided by the Université du Québec à Montréal (UQAM), was  
116 situated at the confluence of the Madawaska and Saint John rivers for the IOP during April and May 2021. The  
117 MUST was located on property provided by the City of Edmundston and was used as a base for graduate students  
118 and volunteers to record manual observations, capture macrophotography images of hydrometeors, and release  
119 sounding balloons for upper air observations. Finally, community volunteers were engaged by providing locations  
120 for either a satellite dish associated with the Smart Rainfall System (SRS) array (Coli et al., 2019), or a  
121 precipitation gauge and snow board for the Community Collaborative Rain, Hail, and Snow Network  
122 (CoCoRaHS) (Cifelli et al., 2005). Furthermore, 10 grade 6 classes (11-12 years old) from local elementary  
123 schools also enrolled as CoCoRaHS observers.

### 125 **2.2 Precipitation Phase Observatory**

126 The Precipitation Phase Observatory (henceforth, the Fixed Station) encompassed a semi-permanent array of  
127 meteorological instruments that were installed ~100 m from the Edmundston ECCC station on 30 November 2020  
128 (Table 1, Figs. 1 and 2). The site was situated at the southern end of an area of open grassland in a broad valley,  
129 152 m above sea level (ASL). The valley is 120-200 m wide by 1 km long, oriented north-south, and bordered by  
130 coniferous forest. The 14-ha site acts as the municipal aquifer resupply and was provided by the city of  
131 Edmundston for the installation. We provide specific location details in Table 1. This site was chosen to allow for  
132 the SAJESS datasets to be supplemented [and compared](#) with records from the nearby ECCC station, [which was](#)  
133 [comprised of a Geonor T-200B](#) weighing precipitation gauge [with a single Alter shield, three sonic ranger snow](#)  
134 [depth sensors, three Temperature/RH probes, and a RM Young wind monitor atop a 10-m mast.](#) Additionally, the

135 open field provided an opportunity to install an Infrared Gas Analyzer and Sonic anemometer (IRGASON) to  
136 estimate surface turbulent fluxes and compute surface energy balances (Table 2) during the IOP (see Section 2.2).  
137



138  
139 **Figure 2: The Precipitation Phase Observatory instrumentation, image taken looking north. From left-to-right: The**  
140 **K63 Hotplate, a laser-optical disdrometer installed upon the meteorological tripod, and the Micro Rain Radar. This**  
141 **station was also to be known as the ‘Fixed Station’. Picture taken 1 December 2020.**

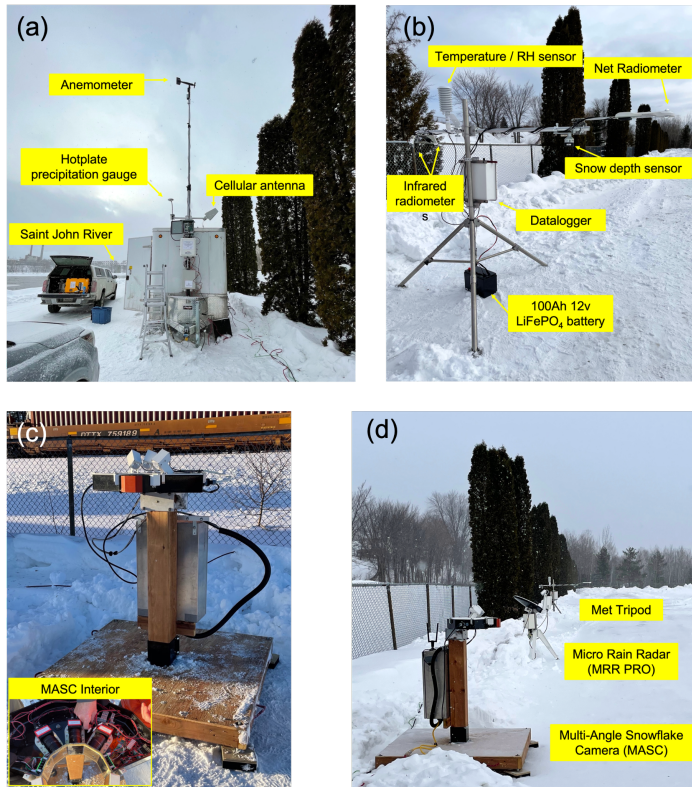
142  
143 The identification of precipitation phase was achieved at the Fixed Station by the installation of a laser-optical  
144 disdrometer for recording particle size and fall speed, and by a vertically pointing micro rain radar (MRR) to  
145 provide information on the atmospheric conditions aloft (see Section 3 and Table 2). A K63 Hotplate Total  
146 Precipitation Gauge (henceforth, hotplate) was installed to measure precipitation rate and amount. Aside from  
147 periods of missing data (~5%), the Fixed Station dataset, excluding the Flux Tripod (see Section 3.1.2), spans 1  
148 December 2020 – 30 April 2021.

### 149 2.3 Intensive observation period

150 Due to limitations at the Fixed Station (e.g., no fuel or generator use), a separate IOP site was established so that  
151 the Mobile Urban Weather Station Trailer (MUST) and instruments could frequently be visited by observers (Fig.  
152 1). The 6' × 12' enclosed trailer was equipped with heating, AC power, helium cylinders, and instrument storage;  
153 it was parked on a fenced parcel of land on the north bank of the Saint John River and the east bank of the mouth  
154 of the Madawaska River, 143 m ASL. Although the 3.3-ha site is dominated by the Edmundston wastewater

**Deleted:** K63 Hotplate Precipitation Gauge (henceforth, hotplate) to measure precipitation rate and amount, a  
**Deleted:** to discern particle type and record

158 ponds, there was sufficient space for the MUST Trailer and instrumentation to be placed along the northern edge  
159 of the site (Figure 4).



160  
161 Figure 3: Instruments and sensors co-located with the Mobile Urban Station (MUST) trailer. (a) The MUST trailer  
162 with extended 10 m mast, anemometer (not included in the dataset), and K63 Hotplate, (b) the meteorological tripod,  
163 (c) the Multi-Angle Snow Camera (MASC) with a top-down view of the internal components and three high-speed  
164 cameras, and (d) the MASC, MRR Pro, and meteorological tripod lined along the access road to the water treatment  
165 lagoon. Pictures taken 3 March 2021.

166

167 The proximity of the instruments to the open ponds, nearby railway, and urban environment, resulted in the focus  
168 on manual observations of weather conditions and precipitation type, rather than automated instrumentation, at  
169 this location. We therefore stationed equipment that required regular attention or manual operation, such as the  
170 multi-angle snowflake camera (MASC) (Figure 3c) and macrophotography equipment (not shown). Manual  
171 observations and macrophotography (see Section 3.2) were conducted at the site from 1 March 2021 – 27 April  
172 2021.

### 173 2.3 Smart Rainfall System (SRS)

174 The Smart Rainfall System (SRS) was installed at six sites in the Edmundston area to capture the spatial variability  
175 of precipitation by exploiting the satellite-to-earth links technology (Colli et al., 2019). Some locations were also  
176 chosen to provide measurements upstream and downstream of Edmundston. The SRS system uses a standard  
177 parabolic dish to receive satellite telecommunication broadcasting signals and an algorithm converts the signal  
178 attenuation to precipitation rate (section 3.4). Locations with parabolic dishes that were already installed by  
179 community volunteers for telecommunication purposes, but not being used during the experiment period, were  
180 selected. Locations are shown Fig. 1.

Deleted: several

### 181 2.4 Community involvement (CoCoRaHS)

182 While the CoCoRaHS network provides a broad array of precipitation measurements across North America  
183 (Reges et al., 2016), there were few CoCoRaHS observer sites in the SAJESS study region. With assistance from  
184 CoCoRaHS Canada (Colorado Climate Center, 2017), SAJESS students and staff facilitated the distribution of  
185 equipment and training to a total of 21 new CoCoRaHS stations (Table 4), including 10 elementary schools, during  
186 the 2020-2021 winter season. CoCoRaHS site metadata available to the public can be found at  
187 <https://cocorahs.org/Stations/ListStations.aspx>.

## 188 3. Field instruments and manual observations

### 189 3.1 Instrumentation

190 The main consideration when deploying instruments to SAJESS was how to measure the amount, phase, and type  
191 of precipitation that occurs during the winter and spring seasons. Particular attention was paid to gathering data  
192 throughout as much of the tropospheric column as possible.

193

195 Here we provide an overview of the instrumentation used during SAJESS. Sensor details, parameters, and units  
196 are included in Tables 2 and 3. [Further](#) details of each sensor, [such as the date of manufacture, last calibration,](#)  
197 [and serial number](#), are also provided [in the readme files](#).

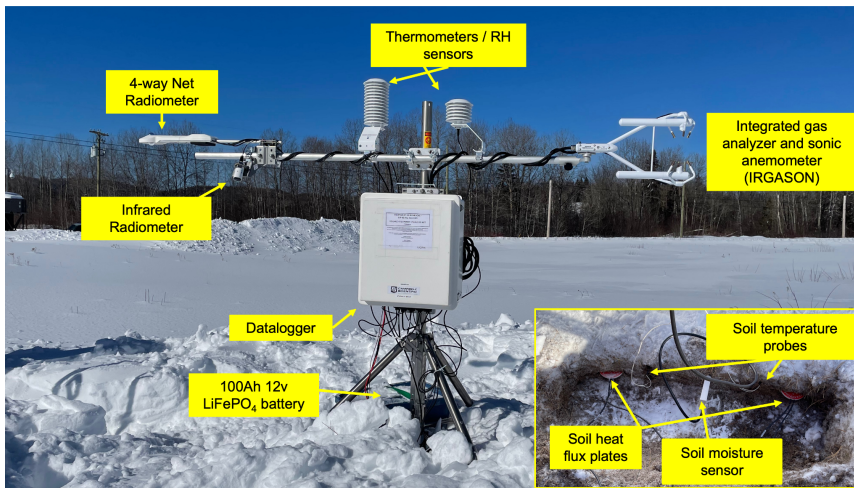
### 198 3.1.1 Meteorological tripod

199 Standard meteorological variables were measured at each of the two main sites. Common parameters for  
200 each site were 2-m air temperature and relative humidity, 4-way net radiation (upwelling and downwelling  
201 long-wave and short-wave radiation, LW↑, LW↓, SW↑, and SW↓), surface temperature, and snow depth.  
202 Measurements at the Fixed Station also included soil surface temperature and moisture content. Snow at the  
203 Fixed Station remained undisturbed for the winter and total snow depth was recorded continuously for  
204 December 2020 – April 2021. Due to disturbance of the snowpack surrounding the MUST Trailer by foot  
205 traffic, [vehicles](#), and [the](#) installation of other instruments, a 30 cm × 30 cm white snow board was placed  
206 underneath the snow depth sensor and cleared after each significant snowfall event. [The clearing of the snow](#)  
207 [boards was consistently performed by the volunteers/students. They were cleared at the beginning of observations](#)  
208 [before precipitation started, then cleared again once precipitation ended. Through these actions, the ensuing data](#)  
209 [should be considered by users as a snowfall measurement rather than true snow depth.](#) On each met tripod, the  
210 snow depth sensor was installed on the south end of the tripod cross arm so that the legs of the tripod would not  
211 be within ~1 m diameter cone of detection. For surface temperature, two infrared radiometers (IRRs, henceforth  
212 IRR 1 and IRR 2) were mounted to the north end of the cross arm of each met tripod and angled away ~ 30  
213 degrees. At the Fixed Station, IR 1 faced slightly west, while IR 2 faced slightly east. At the MUST Trailer site  
214 these were reversed. The net radiometer and snow depth sensors were mounted on the south end of each cross  
215 arms.

### 216 3.1.2 Flux tripod

217 An Open-path Eddy Covariance system was installed at the Fixed Station for the IOP from 5 March 2021 to 30  
218 April 2021. The integrated Infrared Gas analyzer and Sonic Anemometer (IRGASON), temperature/RH probe,  
219 net radiometer, infrared radiometer, soil probes, and heat flux plates were installed following the prescribed  
220 methods found in Campbell Scientific (2022a), with the IRGASON sensor facing north into the prevailing wind.  
221 Winds (in 3-D), air temperature, ambient pressure, and CO<sub>2</sub> and H<sub>2</sub>O densities were captured at 10 Hz resolution  
222 and averaged over 30 minutes to calculate turbulent fluxes and energy closure balances (Campbell Scientific,

223 2022b). The dataset also includes diagnostic data, data quality values, and coefficients used for the eddy-  
224 covariance calculations during each 30-min period so the raw time series data can also be post-processed using a  
225 variety of software (US Department of Energy, 2022).  
226



227  
228 **Figure 4: The Fixed Station flux tripod. An open-path eddy-covariance system consisting of an Infrared Gas Analyser**  
229 **and Sonic Anemometer (IRGASON), soil temperature probes, a soil moisture sensor, a net radiometer, an infrared**  
230 **radiometer, and temperature/RH sensors. This tripod was installed for the melt period from 5 March to 30 April 2021.**  
231 **Picture taken 5 March 2021.**

### 232 3.1.3 Hotplate precipitation gauge

233 A hotplate precipitation gauge (henceforth, hotplate) was installed at the eastern end of the Fixed Station  
234 instrument array (Fig. 3) (Rasmussen et al., 2011; Thériault et al., 2021b). As outlined by Cauteruccio et al. (2021),  
235 the hotplate was tested during the World Meteorological Organization’s Solid Precipitation Intercomparison  
236 Experiment (SPICE) (Nitu et al. 2018), and the Global Precipitation Measurement Cold Season Precipitation  
237 Experiment (GCPEX) (Skofronick-Jackson et al. 2015). The hotplate measures liquid-equivalent precipitation by  
238 recording 1-minute and 5-minute running averages of precipitation rate and wind speed (needed as control for  
239 precipitation rate). An accompanying environmental sensor measures air temperature, RH, and atmospheric  
240 pressure with the same 1-minute and 5-minute temporal resolution. SAJESS was the first time in Canada that the



241 Pond Engineering version of the hotplate was used in a field campaign. A second one of this type of hotplate was  
242 installed for the IOP on the MUST Trailer mast and is detailed in Section 3.1.7.

#### 243 **3.1.4 Disdrometer**

244 A laser-optical disdrometer was deployed at the Fixed Station for the duration of the field campaign on the same  
245 tripod as the standard meteorological instruments, at 2.8 m AGL (Fig. 3). [The disdrometer provides measurements](#)  
246 [of the size and speed of falling hydrometeors which, when post-processed accordingly, can provide a classification](#)  
247 [of hydrometeor type \(Hauser et al., 1984; Rasmussen et al., 1999; Löffler-Mang and Joss, 2000; Ishizaka et al.,](#)  
248 [2013; Thériault et al., 2021a\). Included in the dataset are variables derived by the manufacturer's software such as](#)  
249 [precipitation intensity \(mm h<sup>-1</sup>\), number of detected particles, and several national standard present weather](#)  
250 [codes. The spectrum of particles is provided by 1024 columns representing the 32 × 32 matrix of particle fall](#)  
251 [speed and diameter bins. The mid-values and spread of these bins are listed in the readme file supplied with the](#)  
252 [dataset and in the disdrometer user manual \(OTT, 2019\).](#)

#### 253 **3.1.5 Micro Rain Radar**

254 A micro rain radar (MRR) at each of the primary sites was used during SAJESS to vertically profile hydrometeor  
255 reflectivity and Doppler velocity (Tokay et al., 2009; Souverijns et al., 2017). A METEK MRR-2 was installed at  
256 the Fixed Station, 2.6 m AGL, at the western end of the instrument array (Fig. 3). [The MRR-2 has 32 range gates](#)  
257 [\(height steps\) and we set the height resolution to the maximum of 200 m, giving a maximum height of 6400 m.](#)  
258 Raw data from the MRR-2 were post-processed using the IMProToo algorithm from Mahn and Kollias (2012), as  
259 outlined in Thériault et al. (2021a). [An MRR-Pro was installed at 1.3 m AGL at the MUST Trailer \(Fig. 4d\).](#)  
260 [Settings for the MRR-Pro were: 128 range gates, 64 spectral lines, 10 s sampling, 50 m height resolution, and](#)  
261 [6350-m ceiling. The combination of these parameters results in a velocity range of 12 m s<sup>-1</sup>, and a velocity](#)  
262 [resolution of 0.19 m s<sup>-1</sup>. The 10 s averaging time results in a total of 305 spectra being averaged for each](#)  
263 [measurement.](#) Both radar units used built-in dish heating to eliminate snow and ice build-up during precipitation  
264 events.

#### 265 **3.1.6 Multi-Angle Snowflake Camera**

266 A multi-angle snowflake camera (MASC) was installed at the MUST Trailer (Fig. 4c and d), on a wooden stand  
267 ~1.4 m above the ground, for the majority of the IOP (5 March 2021 – 27 April 2021). Accumulating snow around  
268 the base of the stand was removed by students to prevent the re-suspension of previously captured particles (Fitch



269 et al., 2021; Schaer et al., 2020). The MASC consists of three high-speed cameras housed in a single enclosure,  
270 with 36° separation between each camera, and a focal point ~10 cm for each lens. The cameras take images  
271 simultaneously when particles are detected within a ring-shaped viewing area (Fig. 4c inset). The three images  
272 from each trigger consequently show the hydrometeor(s) from slightly different angles. First introduced by Garret  
273 et al. (2012), MASCs have been deployed in Antarctica (Praz et al., 2017), the Colorado Rockies (Hicks &  
274 Notaros, 2019), and Alaska (Fitch et al., 2020). Images have been used individually to illustrate the hydrometeors  
275 observed, and highlight the riming conditions, crystal habit, size of particles.

Deleted: Garrent

### 276 3.1.7 MUST Trailer mast

277 A telescopic pneumatic 10-m mast attached to the MUST trailer supported an anemometer and wind vane (at 10  
278 m), a hotplate precipitation gauge at 3.5 m, and the antenna for upper air observations (see Section 3.3) (Figure  
279 4a). Due to air leakage, the mast did not always maintain its full extension and therefore required re-extending at  
280 times. This, in addition to the proximity of the trailer to trees and a nearby structure has resulted in us excluding  
281 the wind data from the publicly available dataset.

### 282 3.2 Macrophotography, manual observations, and timelapse images

283 Observers were present at the MUST Trailer during periods of precipitation to report weather conditions, and to  
284 obtain macrophotographs of solid hydrometeors (Gibson and Stewart, 2007; Joe et al., 2014; Thériault et al., 2018;  
285 Lachapelle and Thériault, 2021a). This provided a running-record of the weather conditions during storm events  
286 and allowed for the field-training of students in manual observations, and identification of precipitation types and  
287 snow crystal habits. The recording of manual observations can also remove doubt about precipitation arriving at  
288 the surface. This is especially important with respect to hydrometeor type during periods of near-freezing  
289 conditions, during which a mixture or changes in precipitation phase or type can occur. This also reduces the  
290 potential for misdiagnosis by instrumentation or modeling. Observations of sky condition, cloud type, and  
291 precipitation type (solid, liquid, or mixed), and images from a digital single lens reflex (SLR) camera fitted with  
292 a macro lens and ring flash, were taken every 10 min. Precipitation was collected on a black velvet collection pad  
293 during a short period (5 - 30 seconds), depending on the precipitation rate. The aim was to ensure that there were  
294 enough particles to represent the precipitation conditions, while avoiding particles overlapping each other. The  
295 collection pad was wiped every time after the series of nine images were taken using a set sequence of movements  
296 of the camera upon a sliding frame. Images of a ruler placed across the pad for scale were taken intermittently,  
297 for example when the camera was removed/replaced on the stand. Users can assume the scale remains constant

299 [between these images \(each image is 2 cm across\). The scale images are listed in the macrophotography readme](#)  
300 [file. More details of the method, including images of the equipment, can be found in Thériault et al. \(2021a\) and](#)  
301 [Thériault et al. \(2018\). Other conditions to note](#) were the occurrence of very light precipitation which can be  
302 missed by disdrometers, and the presence of blowing snow that could affect analysis of MASC data (Section  
303 3.1.6).

304  
305 Hourly images of each site, including the surface conditions around the instruments, were captured by a time lapse  
306 camera. [Similar previous campaigns by the authors have found time-lapse images to be very useful in confirming](#)  
307 [sky and surface conditions such as snow-on-the-ground onset and they have also provided evidence of wildlife](#)  
308 [encounters with the instrumentation. Precipitation type diagnoses, however, are not usually possible with these](#)  
309 [images.](#)

### 310 **3.3 Upper air observations**

311 Soundings were timed to coincide with [the standard synoptic times of 00, 03, 06, 09, 12, 15, 18, or 21 UTC. Some](#)  
312 [additional launches were attempted to coincide with precipitation phase transitions. Sonde retrieval was not](#)  
313 [attempted during this experiment.](#) A total of 52 balloons were launched from the MUST Trailer and [we include](#)  
314 [text files for 46 of those launches that](#) resulted in a complete sounding of the troposphere from which profiles of  
315 pressure, temperature, dew point and winds (speed and direction) can be produced. [Files of each sounding are also](#)  
316 [available from the authors in other commonly used sounding formats.](#)

### 317 **3.4 Smart Rainfall System**

318 SAJESS served as the opportunity to deploy an innovative environmental monitoring technique, the Smart  
319 Rainfall System (SRS), that has been developed by the University of Genoa, Genoa, Italy and currently distributed  
320 by Artys srl. The SRS produces estimations of liquid precipitation, in 1-min rainfall intensity, by processing the  
321 attenuation of the satellite microwave link (SML) signal emitted by commercial geosynchronous satellites for  
322 Digital Video Broadcasting (DVB-S) and received by common parabolic antennas (Colli et al., 2019). Estimating  
323 liquid precipitation using the SRS has been confirmed by several experimental initiatives (Giannetti et al., 2021).  
324 In contrast, snowfall intensity retrieval at centimeter wavelengths (the DVB-S signal is transmitted in the Ku  
325 frequency band) is more uncertain. It has been demonstrated that higher operating frequencies, and preferably  
326 dual-band systems, are needed to successfully retrieve solid precipitation (Falconi et al., 2018; Liao et al., 2016).

327

328 SAJESS provided the experimental conditions for SRS devices to monitor the liquid content in cases of mixed  
329 precipitation and wet (melting) snow. The SRS system tested in Edmundston was composed of a set of distributed  
330 SML sensors, as described by Colli et al. (2019), connected to a central processing and analysis node to reconstruct  
331 the bi-dimensional rainfall field in real time. To an onlooker, the only equipment visible is a small box placed  
332 inside the residence that connects inline to the satellite dish coaxial cable. The processor inside the box is then  
333 configured to connect to the local Wi-Fi network. To reduce signal noise, it is preferable that the satellite dish no  
334 longer be in service. These results will be published once work is complete.

**Deleted:** The SAJESS experiment represents the first operational use of the SRS for monitoring

### 335 3.5 CoCoRaHS sites

#### 336 3.5.1 CoCoRaHS gauges and snowboards

337 Volunteers from the community and local elementary schools contributed to SAJESS by recording meteorological  
338 measurements for the CoCoRaHS network (Cifelli et al., 2005). This provided an opportunity for students to  
339 engage in the data collection process, and to learn about the importance (and difficulties) of precipitation  
340 determination. A typical CoCoRaHS station includes a manual precipitation gauge to measure liquid and solid  
341 precipitation, and a 40 cm × 40 cm white board for measuring snow depth. Daily measurements include the amount  
342 of precipitation, depth of snowfall, and snow water equivalent (SWE). Weekly measurements consist of total snow  
343 depth, and the total SWE. CoCoRaHS data can be found using the network's online database; station details are  
344 provided in Table 4. In addition to the regular CoCoRaHS station equipment, some volunteers hosted dataloggers  
345 to record air temperature and relative humidity (see below).

#### 346 3.5.2 Temperature sensors

347 HOBO MX2301A data loggers were distributed to 13 community volunteers (Fig. 1, Table 4), and correct  
348 installation of each sensor was confirmed by a SAJESS team member. Installed approximately 2 m above the  
349 ground, the dataloggers measure air temperature and relative humidity every 5 minutes (Onset Computer  
350 Corporation, 2022). These low-cost, robust sensors provided a broad (50-60 km) network to assess spatial  
351 variability in near-surface temperature/RH, especially during the passage of fronts and the onset/cessation of  
352 precipitation. Data were retrieved from the HOBO devices via a Bluetooth smartphone app that reduced the need  
353 to handle the sensor.

356 **4 Data description**

357 **4.1 Data processing and management**

358 Here we provide a short summary of the data processing and archiving strategies. Full details on all data, including  
359 specifications of the instruments used, can be found in the readme files uploaded to the FRDR repository.

360

361 Firstly, all instrumentation, camera equipment, observer notes, and computers were set to UTC date and time.  
362 Instruments that produce relatively low-volume text-based data such as the disdrometer, meteorological tripods,  
363 hotplate precipitation gauge, and temperature sensors, have been processed by concatenating smaller files together  
364 to create monthly files. Missing timestamps have been added to ensure every file contains timesteps for each  
365 minute of the month. All missing data points have been filled with NANs and no interpolation of missing data  
366 points has been attempted for the data uploaded to the FRDR repository. For standard meteorological variables  
367 such as temperature, humidity, snow depth, and radiation measurements, values have been quality checked to  
368 ensure they fall within the operating range of each instrument, with values outside of these ranges being set to  
369 NAN.

370

371 Raw radar data (.raw files) from the Fixed Station radar have been processed into daily NetCDF (.nc) format using  
372 the algorithm detailed by Maahn & Kollias (2012). Both .raw and .nc files have been included in this dataset.  
373 Hourly data from the MUST Trailer radar (MRR Pro) have been archived as .nc files as these data are produced  
374 by the instruments embedded processor (METEK, 2017)

375

376 Photographic images have not been altered or cropped and are uploaded as .png files for the MASC and  
377 macrophotography, or .jpg files for the timelapse cameras. Manual observations recorded in spreadsheets have  
378 been archived as comma separated value (.csv) files. Upper air observations are saved as one file per sounding, in  
379 tabular-delimited files, indexed by UTC date and time at a temporal resolution of 1 second.

380

381 In most instances, files have been identified using a specific naming convention using abbreviations for the project  
382 (SAJESS, SJ), each site (Fixed Station, FS; MUST Trailer MT), and each instrument (see Tables 2 and 3). For  
383 example, data from the disdrometer at the Fixed Station for the month of January 2021 are contained in the file:  
384 SJ\_FS\_DIS\_MAS\_202112.txt. (The abbreviation MAS stands for master and is used by the field staff to identify  
385 data that have been assembled ready for upload to the repository). MASC images do not follow this naming

Deleted: in-situ

387 convention as the software used with the instrument provides a detailed filename with respect to the snowflake  
388 number and timestamp of the image.

#### 389 **4.2 Data validity**

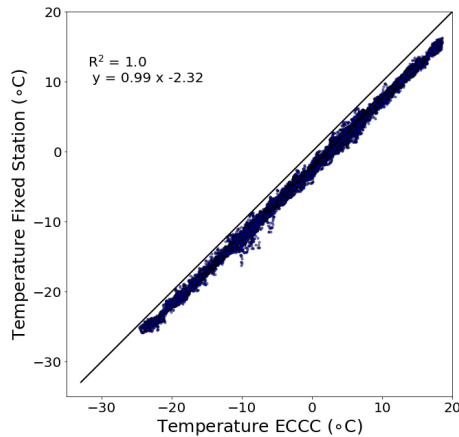
390 While not exhaustive, we list below known issues and attempts to-date at validating data from the SAJESS  
391 instruments and observations. To preserve the raw data recorded during SAJESS, no quality control related post-  
392 processing has been performed. We encourage all users to perform quality control and post-processing according  
393 to their needs. We invite users to contact us for further information as several projects using SAJESS data are  
394 ongoing.

##### 395 **4.2.1 Met Tripod**

396 To our knowledge the only instrument to suffer from a systematic error was the HMP155A temperature and  
397 humidity probe located on the meteorological tripod at the Fixed Station. Incomplete grounding at the datalogger,  
398 and the subsequent datalogger program, resulted in a bias of  $\sim -2.32^{\circ}\text{C}$  when compared to temperature data from  
399 the ECCC station (Fig. 5). Due to the uniform pattern of the bias resulting in a low RMSE, these data have been  
400 retained in the dataset and are available for use. Correction of these data by  $+2.32^{\circ}\text{C}$  in on-going snow modeling  
401 analyses indicate these data are still useful if post-processed accordingly. Post-deployment testing indicates that  
402 this bias is not present in the temperature data from the MUST Trailer met tripod.

403  
404 While data from the hotplate precipitation gauge include air temperature and humidity that align well with the  
405 ECCC station (i.e., do not require bias correction), these data have significantly more noise than data from the  
406 meteorological tripod sensor.

407



408  
 409 **Figure 5: SAJESS Fixed Station and ECCC temperature data. Comparison of 1-minute temperature data (63149**  
 410 **recordings) from the Fixed Station temperature probe and the mean of the three ECCC temperature thermistor**  
 411 **readings. The Fixed Station HMP155 has a -2.32 °C bias due to the method of wiring and data recording.**

412  
 413 Analysis of the IRR surface temperature data indicates that shading from the tripod and datalogger enclosure may  
 414 have affected these measurements. When snow was present, the side with a shaded field of view (west in AM,  
 415 east in PM) measured warmer conditions (up to ~2°C) than on the unshaded side. Once snow cover was absent,  
 416 the trend was reversed so that the shaded side is cooler (up to ~6°C). This diurnal pattern of temperature difference  
 417 between the two sensors existed at both SAJESS locations, so we caution against the averaging of both sensors  
 418 without taking these differences into account. We found similar results to Domine et al. (2021) where RMSE  
 419 between the net-radiometer (using LW↑), and the IRRs was best reduced using an unphysical emissivity ( $\epsilon$ ) value  
 420 of 1.028. This could indicate that direct comparison is difficult due to the difference in wavelength spectrum  
 421 measured by the two instruments (Domine et al., 2021), yet the greater field of view of the net radiometer may  
 422 also be influential. Surface temperature data have not been corrected for surface emissivity, and assume  $\epsilon = 1$   
 423 (Apogee Instruments Inc., 2022). The location of the IRRs should be installed on the unshaded south end of the  
 424 cross arm in future deployment.

**Deleted:** Although the 4-way net radiometer provides LW↑,

427 [Snow depth measurements](#) from the [sonic ranger \(SR50A\)](#) on the Fixed Station meteorological tripod were within  
428 10% of the values from the same type of sensor used by ECCC at the Edmundston station over the course of the  
429 2020-21 winter. At both SAJESS sites, the 1-min resolution caused noise in the snow depth data during periods  
430 of precipitation, which is greatly reduced using a 1-hour running mean. Data from the SR50A also include a  
431 'quality number', which is detailed in the dataset readme and can be used to filter snow depth data.

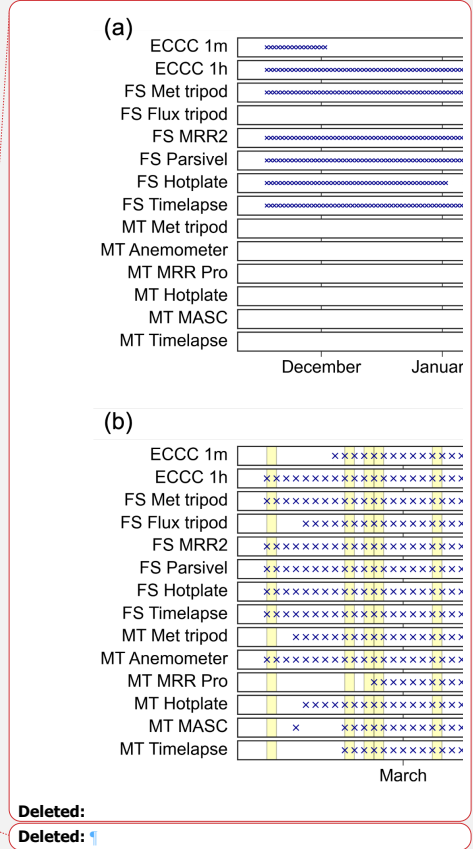
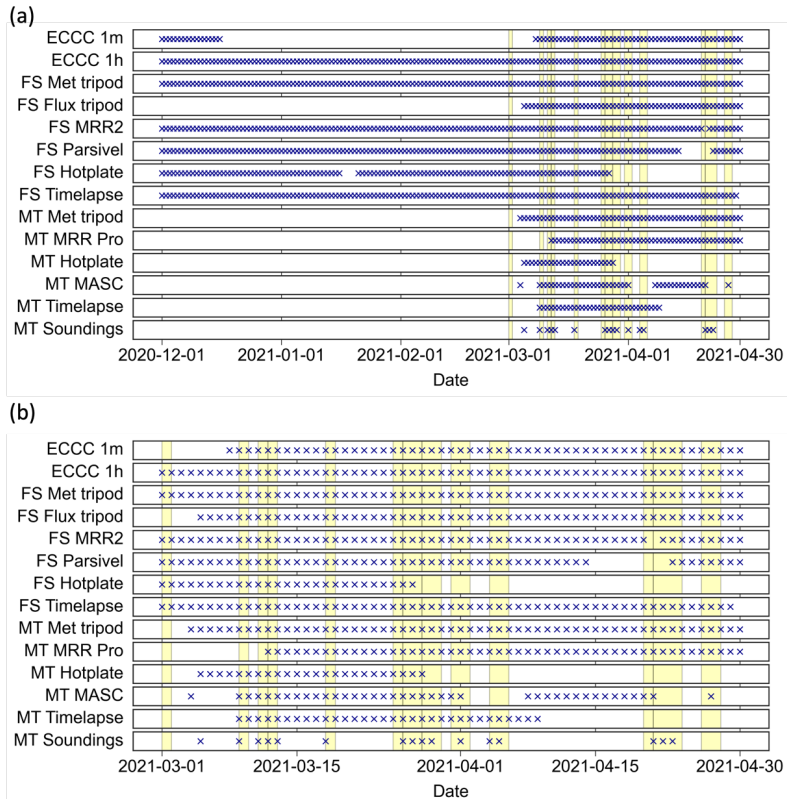
432

433 The 4-way net radiometers on each meteorological tripod were fitted with the heater/ventilation unit to  
434 reduce errors associated with dew/frost on the sensor window. This unit, however, does not heat the sensor  
435 window(s) sufficiently to remove snow or ice during or after precipitation, which is observed in the  
436 pyranometer data when  $SW\uparrow$  is greater than  $SW\downarrow$ , and correlated with precipitation events using the  
437 disdrometer and/or snow depth data. This situation occurred on 13 days at the Fixed Station and five days at  
438 the MUST Trailer. For data analysis we suggest using more advanced algorithms such as Lapo et al. (2015)  
439 to identify periods of snow accumulation, which can then be corrected with other methods available in the  
440 literature (e.g., Sicart et al., 2006; Annandale et al., 2002). Unlike Domine et al. (2021), no sustained periods  
441 of  $0.0 \text{ W m}^{-2}$  are observed in the  $LW\downarrow$  data, indicating the continuous use of the ventilation unit was  
442 successful in preventing frost build-up.

#### 443 **4.2.2 Flux tripod**

444 Users wishing to utilize data from the flux tripod can investigate variables provided in the Flux Notes (FN),  
445 Campbell Scientific (CS), and AmeriFlux (AM) files. These include the number of [CO<sub>2</sub>](#), H<sub>2</sub>O samples per  
446 averaging period, and a corresponding 'bad data' column. We observe that the maximum number of samples at  
447 10 Hz for the 30-minute period (18,000 in total) did not reach a total of 19.5 hours during the March-April 2021  
448 IOP. These occurrences correspond to periods of precipitation whereby we presume the IRGASON windows were  
449 inhibited by rain/snow. On a finer scale, steady state integral turbulence characteristic (SSITC) tests were applied  
450 to energy balance components for every 30-minute period (Foken et al., 2004). These can be found in the AM  
451 files as variables named '\_SSITC\_TEST', and in the CS files as variables named '\_QC'. Users should consult  
452 Foken et al. (2004) for further information regarding these tests as further analysis is beyond the scope of the  
453 paper. Data have not been gap-filled, removed, or replaced from the dataset.

454



455

456 **Figure 6: Data availability (daily resolution). Operating periods for instrumentation for (a) the entire SAJESS field**  
 457 **campaign, 1 December 2021 – 30 April 2021, and (b) during the intensive observation period, 1 March 2021 – 30 April**  
 458 **2021 (bottom). Data availability for the Environment and Climate Change Canada station in Edmundston is given for**  
 459 **illustrative purposes only, as ECCC data are not included with this dataset. (FS stands for Fixed Station, and MT for**  
 460 **MUST Trailer). Vertical yellow bands indicate periods of manual observations at the MUST Trailer during storm**  
 461 **events by SAJESS volunteers and students.**



#### 464 4.2.3 Hotplate

465 Although the hotplate performed well when fully operational, a significant portion of the IOP was missed (28  
466 March 2021 to 30 April 2021) due to faulty microprocessor settings on both hotplates (Fig 6). These have  
467 subsequently been improved upon by the manufacturer, and further testing is underway. As described by  
468 Rasmussen et al. (2011), hotplate precipitation rate accuracy is least assured during the onset and cessation of  
469 precipitation, however, data from the hotplates include a 'Status' variable (#1, #2, or #3), that identifies these  
470 periods. A full explanation is provided with the dataset readme. Precipitation data from the hotplate have not been  
471 corrected for these under- or over-estimations.

472  
473 Similar to Thériault et al. (2021b), we compared 30-minute cumulative sums of the hotplate 1-minute  
474 accumulation for Dec 2020 – March 2021, with corrected Geonor data (using Kochendorfer et al., 2017) from the  
475 Edmundston ECCC station. These align well with the best results (reduced bias and RMSE) found for rain ( $>2^{\circ}\text{C}$ )  
476 and snow ( $<-2^{\circ}\text{C}$ ). Finally, hotplate T1 (1-minute average) precipitation data are more sensitive and therefore  
477 better at reproducing higher precipitation rates than the T5 (5-minute average) data, resulting in a positive bias up  
478 to  $\sim 1.5 \text{ mm h}^{-1}$  (at  $4\text{--}5 \text{ mm h}^{-1}$ ).

479  
480 Due to processor issues, barometer data were not recorded by the hotplate environmental sensor at all 1- or 5-  
481 minute intervals, however, valid readings do exist for each hour of the campaign. We recommend filtering  
482 barometer data from both SAJESS sites by selecting the median value during each hour to represent the hourly  
483 value. This method correlates well with ECCC station pressure reading (within 4 hPa) for the duration of the  
484 campaign. Barometer readings represent raw station pressure and are not corrected for elevation.

#### 485 4.2.4 Disdrometer

486 The disdrometer dataset contains 1024 columns, which includes total particle counts and fallspeed, particle  
487 spectrum (Section 3.1.4) and other derived variables listed in Table 4. This configuration option is provided by  
488 the OTT software as raw data. At present we can only comment on a preliminary analysis of the OTT-derived  
489 precipitation intensity. When compared to 30-minute ECCC Geonor and hotplate precipitation rates, timing and  
490 amounts from the disdrometer are generally comparable, yet we observe the Parsivel<sup>2</sup> overestimates at high  
491 precipitation rates ( $>10 \text{ mm hr}^{-1}$ ), which is well documented (e.g., Angulo-Martínez et al., 2018). Users wishing  
492 to utilize the drop size and fall speed distributions, and subsequently retrieve an improved precipitation rate, can  
493 correct these data using Raupach and Berne (2015).

494 **4.2.5 Upper air observations**

495 Comparisons from four soundings from the MUST Trailer that aligned with either the 1200 UTC or 0000 UTC  
496 balloon releases from Caribou (ME) were made for data from 18, 27, and 29 March 2021, with all four sounding  
497 profiles displaying good agreement between the two sites. On some occasions, surface, and lower troposphere  
498 (<700 hPa) temperatures at Edmundston were up to 5°C cooler than in Caribou, ~60 km to the northwest. The  
499 SAJESS sounding data also correlate well with the surface observations of precipitation type and phase. We  
500 recommend smoothing the 1 s sounding data using a low pass filter (e.g., 10 s running mean) to remove noise in  
501 the temperature and dewpoint profiles.

502 **4.2.6 CoCoRaHS precipitation reports**

503 CoCoRaHS volunteers conducted most of their observations during the IOP, due to the delays in obtaining  
504 equipment and training due to public health measures in place at the time. Despite this, 21 CoCoRaHS stations  
505 (Table 4) reported 1715 daily total precipitation (liquid equivalent) measurements, 1729 new snow measurements,  
506 and 1123 total snow measurements (Fig. 7). A comparison of the daily precipitation and new snow amounts has  
507 not been conducted, but the total snow (i.e., snow on the ground) compares well with the Fixed Station and ECCO  
508 instruments. CoCoRaHS data are not included in the SAJESS dataset as: (a) CoCoRaHS already provide long-  
509 term storage and data retrieval via its own website, and (b) the authors encourage users to explore the CoCoRaHS  
510 database for stations that may be useful for their own analysis that were not associated with SAJESS.

511

512 **4.2.7 MASC**

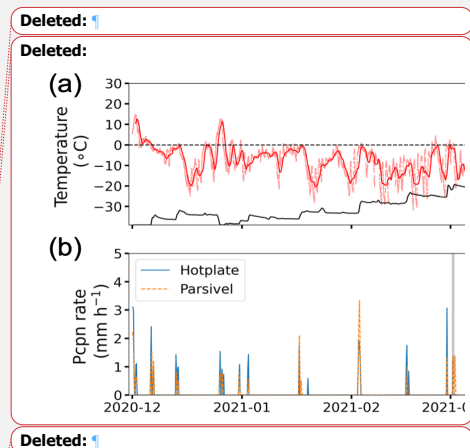
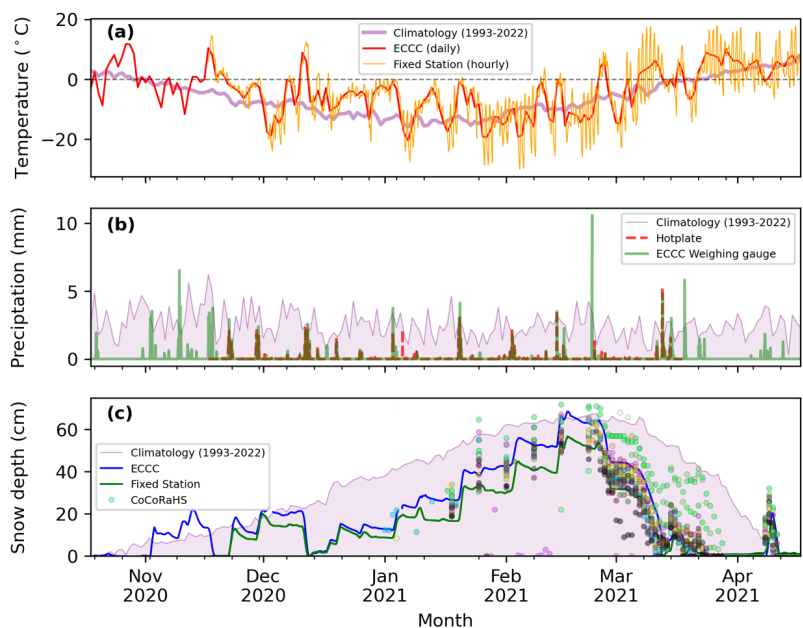
513 The MASC captured a total of 93,343 during March-April 2021. We present some of these images in Section  
514 4.3.3, where they corroborate the particle type recorded by the manual observations. The MASC also allowed for  
515 automated photography of particles when observers were not able to attend to manual observations or  
516 macrophotography. Users should expect, however, a large portion (perhaps 50%) of images to not contain particles  
517 distinguishable to the naked eye. We attribute this to SAJESS representing an experimental opportunity to deploy  
518 the MASC in mixed-phase precipitation conditions. While images of liquid or freezing precipitation were usually  
519 blurred and would be considered less than ideal from an aesthetic point of view, post-processing of the images  
520 using algorithms provided in Praz et al. (2017) has resulted in particle fall speed and size distributions (similar to  
521 disdrometer results) that align well with the observed precipitation type. Analysis of the images is ongoing.

522 **4.3 Examples of data and observations**

523 Here we provide [an overview of the conditions observed during the SAJESS campaign](#), and examples of data  
524 from each of the two SAJESS sites to illustrate possible uses. While the total SAJESS dataset is ~200 Gb, a ~1.1  
525 Gb sample of data is available on the FRDR repository. This sample dataset is based on the example given here  
526 for the MUST Trailer location, where a subset of data for 18 March 2021 is displayed. Sample data have been  
527 made available for most instruments for the entire day (0000 – 2359 UTC), and for the MASC, macrophotography  
528 images, and the MRRs for 1200 – 1300 UTC 18 March 2023 (to reduce file size).

529 **4.3.1 Overview**

530 Data covering [1 December 2020 – 30 April 2021](#) are provided by the instruments at the Fixed Station, [which](#) can  
531 be supplemented [by the near-by ECCC station](#). Maximum snow depth measured at the Fixed Station was 65 cm,  
532 with snowfall amounts comparing well in timing, yet slightly less in magnitude (around 10%), than measured [by](#)  
533 [the ECCC instruments \(Figure 7\)](#). [Maximum snow depth observed at 21 surrounding CoCoRaHS stations \(Table](#)  
534 [4\) ranged from 50 cm to 79 cm, with an average of 54 cm. During this period, the ECCC Geonor measured a total](#)  
535 [of 287 mm of \(liquid equivalent\) precipitation, less than the climatology \(1993-2022\) mean of 364 mm.](#)



536

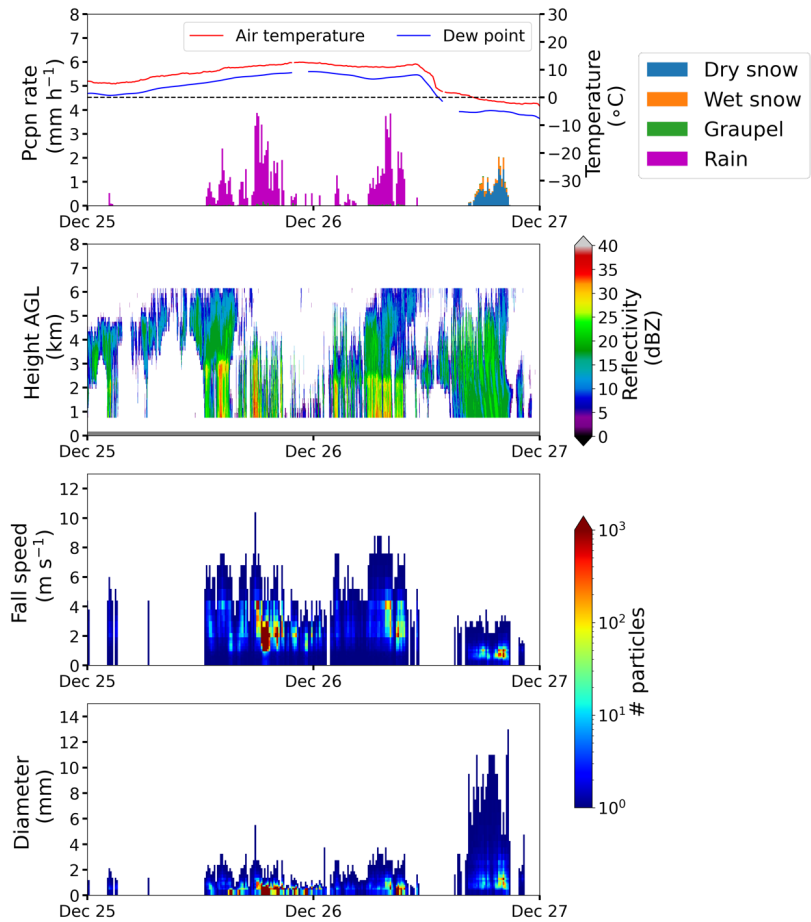
537 **Figure 7: Overview of select SAJESS measurements (December 2020 to April 2021) with comparison to the**  
 538 **Edmundston ECCCC station and 1993-2022 climatology. (a) Hourly mean Fixed Station temperature (corrected, see**  
 539 **Section 4.2.1), daily mean ECCCC temperature, and daily mean climatology temperature. (b) Hourly accumulation from**  
 540 **the Fixed Station hotplate precipitation gauge and ECCCC weighing gauge, with daily climatology accumulation. (c)**  
 541 **Fixed Station and ECCCC snow depth measurements, 1993-2022 snow-on-the-ground climatology, and measurements**  
 542 **from local CoCoRaHS stations listed in Table 5 (each station has a randomly assigned individual marker color). No**  
 543 **hotplate measurements are available, or therefore shown, for April 2021 due to an instrument fault.**

544

545 During the IOP (8 March 2021 - 30 April 2021) manual observations were made during 13 storms (Fig. 6), for a  
 546 total of 183 hours of precipitation-type observations. Observers were present for 93 hours of snow (8 storms), 63  
 547 hours of rain (5 storms), and 27 hours of mixed precipitation (more than one phase of precipitation occurring at  
 548 the same time; 3 storms). Two storms (12 March 2021; 4-5 April 2021) included rain-snow transitions. Observers  
 549 took a total of 4483 images of precipitation particles during the IOP. Using the ECCCC Geonor, observers were  
 550 present for 97 mm of the 105 mm of (liquid equivalent) precipitation that fell during the IOP period.

555 **4.3.2. Fixed Station storm measurements**

556 Focused examples of the meteorological measurements at the fixed station are given Fig. 8. This case covers the  
557 period 25 – 27 December 2020 during which 22.5 hours of rain-on-snow (14 mm) from 1230 UTC 25 December  
558 to 1100 UTC 26 December 2020, with temperatures of 5°C – 6°C, reduced the Fixed Station snow depth to 0.0  
559 m. This was followed closely by a decrease in temperature to < 0°C and ~4.5 hours of snow (4 cm) from 1630  
560 UTC to 2050 UTC 26 December 2021), restarting the seasonal snowpack from bare conditions. Precipitation type  
561 derived from the disdrometer data correlates well with the decrease in air temperature below 0°C. The time  
562 series<sup>31</sup> of particle type can be constructed from the binned fall speed and diameter measurements and by using  
563 equations in the literature such as Rasmussen et al. (1999) and Ishizaka et al. (2013), or by using the precipitation  
564 type codes produced by the instrument software (Table 2). MRR data show the reduction of melting height  
565 (determined by the sharp vertical gradient of reflectivity) from ~ 3 km AGL to just over ~ 2 km AGL during this  
566 same period. These insights to the evolution of the seasonal snowpack are rare as many standard weather or climate  
567 stations may not have the ability to explicitly identify precipitation types.



568

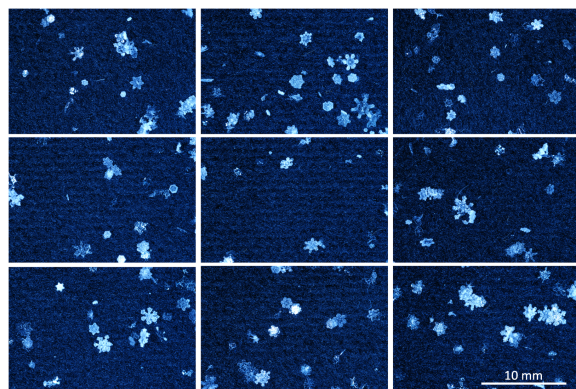
569 Figure 8: Fixed Station storm measurements. From top to bottom, (a) air temperature and precipitation. The  
 570 precipitation type is derived from disdrometer data using equations in Rasmussen et al. 1999 and Ishizaka et al. 2013,  
 571 and is not included in the dataset. (b) radar reflectivity, (c) particle fallspeed, and (d) diameter (both from the Parsivel  
 572 disdrometer), measured at the Fixed Station from 0000 UTC 25 December 2020 to 2359 UTC 26 December 2020.

573 Temperature, dew point, precipitation, and disdrometer data are shown as 10-minute averages. Micro rain radar  
574 (MRR) data are at 10 second resolution, with a vertical resolution of 200 m.

575

#### 576 4.3.3 MUST Station storm observations

577 To complement the automated measurements made at the Fixed Station, the MUST Trailer site provided  
578 observations of precipitation type, photographic imagery of particles, and upper air soundings, [in addition to the](#)  
579 [meteorological tripod and hotplate](#). Images and observations taken during a snow event that occurred on 18 March  
580 2021 are shown in Figs. 9 and 10.



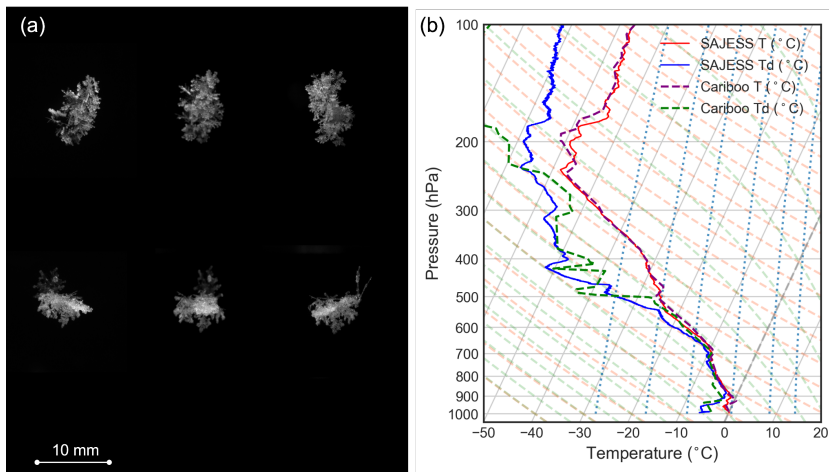
581

582 **Figure 9. MUST Trailer macrophotography. Nine independent (i.e., no overlap) images of the felt-covered pad with**  
583 **solid hydrometeors collected at 1225 UTC 18 March 2021. Images are oriented as they were on the 13 cm × 13 cm pad.**

584

585 [From 1000 UTC to 1430 UTC 18 March 2021, light intermittent snowfall with precipitation rates between 0.4 –](#)  
586 [0.6 mm h<sup>-1</sup> resulted in ~1.5 cm of snowfall at the MUST Trailer. Precipitation rates were at times so low that the](#)  
587 [hotplate did not record any precipitation, but snowfall was confirmed by the manual observations. The Fixed](#)  
588 [Station disdrometer also detected very light precipitation \(maximum rate of 0.6 mm h<sup>-1</sup>\) with only 0.2 mm total](#)  
589 [\(liquid equivalent\) for the same period. The ECCC Geonor did not record any precipitation during this time. Air](#)  
590 [temperature at the MUST Trailer remained between -1°C and 0°C during most of the snowfall, with a short \(~30](#)  
591 [min\) period of snow grains being reported when temperatures increased to 0°C – 0.5°C. Macrophotography](#)

592 images taken from the SAJESS MUST Trailer provide confirmation of hydrometeor type. [From these images](#)  
593 [\(Fig. 9\)](#) crystal habit, size distribution, and riming can be diagnosed, [and they](#) align with the 10-minute  
594 observations that recorded overcast skies, nimbostratus clouds, and snow. Also, during this time, the MASC  
595 captured images of a variety of hydrometeors, with the clearest images being of large aggregates (Fig. 10a). At  
596 1200 UTC 18 March 2021 a deep saturated layer between 900 and 700 hPa is evident on the upper air observations  
597 from the MUST Trailer, matching the vertical profile observed in the National Weather Service (NWS) sounding  
598 from Caribou (ME) (Fig. 10b).  
599



600  
601 **Figure 10. Multi-angle snowflake camera (MASC) images and upper air observations. (a) Two triplet images of**  
602 **aggregates taken by the MASC at 1240 UTC 18 March 2022, and (b) the 1200 UTC 18 March 2021 soundings from the**  
603 **SAJESS MUST Trailer and the NWS Caribou (ME) station.**

604  
605 [After a break in conditions, light precipitation made up of wet snow and rain occurred between 1730 UTC – 1950](#)  
606 [UTC 18 March 2021. The mixed precipitation erased the snow collected on the snowboard under the MUST](#)  
607 [Trailer SR50A. This is important as it illustrates what CoCoRaHS observers would have encountered the next](#)  
608 [morning \(19 March 2021\), when no observations of new snow were recorded.](#)  
609



610 **4.4 Challenges and lessons-learned**

611 Challenges during the SAJESS field campaign primarily originated from the requirement for remote computer  
612 access to monitor and troubleshoot instrument problems as they arose, and intermittent interruptions to AC power,  
613 especially at the Fixed Station site.

614

615 Such issues include the requirement to restart proprietary software. For example, the disdrometer software  
616 provided by OTT requires a user to restart the program manually if the computer has suffered a power interruption  
617 or reboot. This caused some periods of missing data to be longer than necessary. For subsequent deployments we  
618 have circumvented this issue by writing a serial-based terminal program in Python that can run on any operating  
619 system. Conversely, software provided by METEK for the MRR will restart automatically, however, users are  
620 limited to Windows operating software.

621

622 The processor included with the MRR Pro does allow for data collection to begin automatically, for as long as the  
623 on-board hard drive has space, however, raw data then are not retrievable as they are with the MRR2. We found  
624 this to be an adequate trade-off as the longer acquisition time per spectrum results in the MRR Pro signal having  
625 less noise, and due to the larger number of range gates, can have a finer vertical resolution for the same maximum  
626 height as the MRR2. Our use of both versions of the METEK MRR was also due to equipment limitations within  
627 the group.

628

629 A similar restart issue arose for the hotplate, whereby a manual reset was required after the instrument's  
630 microprocessor cut power to the heating plates. This response has been rectified by the manufacturer; however,  
631 we have since installed a remotely controlled AC outlet to our other hotplate stations that can be switched on/off  
632 without having to visit the site in-person.

633

634 SAJESS provided an opportunity to operate the multi-angle snowflake camera (MASC) during mixed-phased  
635 precipitation. Initial results indicate that the instrument can help diagnose mixed-phase precipitation using post-  
636 processing algorithms that diagnose particle fallspeed and diameter to a similar standard as the disdrometer. This  
637 leads, however, to many of the images being of blurred spherical raindrops rather than sharp pictures of ice crystal  
638 types published elsewhere. Work is ongoing to modify the post-processing software to include the categorization  
639 of raindrops, as this category is currently missing from the software.

640

641 Dishes for the SRS are required to be oriented to specific satellites (with the help of a satellite signal finder);  
642 however, it is also best if these dishes are not currently being used to receive a satellite TV signal by the household.  
643 In Edmundston, we located an adequate number of unused dishes within the community, however, an SRS specific  
644 deployment may require the purchasing of new equipment solely for the purpose of the SRS system. In some  
645 regions, satellite dishes may no longer be installed or maintained to a sufficient standard.

646  
647 The use of community-based volunteers to assist in observations at times proved challenging, practically with  
648 respect to data quality. Our conclusion is that SAJESS could have benefited from a smaller number of high-quality  
649 measurements that could be verified, rather than a larger number of measurements that may have been prone to  
650 error. Due to public health measures in place much of the hands-on training that was planned had to be conducted  
651 remotely, and at times restrictions limited the volunteer's access to sites and equipment. We suggest a dedicated  
652 team member to act as liaison for larger groups of volunteers. Compared to the high-temporal resolution of many  
653 of the SAJESS instruments, precipitation amounts recorded once-per-day may not be suitable for all analyses, as  
654 identified in Section 4.3.3.

655  
656 Particularly difficult was the installation of the eddy covariance flux tripod during the winter season. The burial  
657 of temperature sensors and heat flux plates was less than ideal in the frozen surface material, which also precluded  
658 a soil pit analysis and soil layer documentation. However, care was taken to ensure restoration of the soil and turf  
659 was as complete as possible after installation. The overlying snow was also restored as homogeneously as possible  
660 to match the surrounding snowpack. Due to the lack of soil analysis, the datalogger program's default bulk density  
661 value of 1300 kg m<sup>-3</sup> was used. Although future deployments should not underestimate the time and energy  
662 required to install the flux instrumentation correctly, we have retained the flux data as thorough post-processing  
663 has allowed for effective analysis of the data (Leroux et al, 2023).

## 664 5 Summary

665 A valuable dataset was collected during the 2020-2021 Saint John River Experiment on Cold Season Storms  
666 (SAJESS) over Eastern Canada. The dataset contains automatic measurements, manual observations, and photos  
667 of the meteorological conditions and precipitation at the surface, micro rain radar measurements, upper air  
668 observations, and measurements of precipitation amounts by community volunteers.  
669

670 The experiment included an intensive observation period during March – April 2021, to document conditions  
671 during the melt season with its below-average snowpack melt a month earlier than normal. The study region and  
672 downstream communities are historically prone to ice jams and flooding during late winter and early spring, which  
673 can be influenced by air temperature, rain-on-snow events, and the overall evolution of the seasonal snowpack.  
674 Despite these hazards being minimal during the campaign, the dataset will contribute to an understanding of  
675 snowpack evolution across the region by a variety of mechanisms. Firstly, the spatially distributed measurements  
676 from CoCoRaHS observers and SRS installations give a broader view of precipitation types and amounts than the  
677 typical isolated weather or climate station. The dataset contains more than 1700 measurements from these  
678 community volunteers, and the experiment doubled as a learning opportunity for the classes of school children  
679 that contributed by recording snow board and rain gauge measurements. Secondly, the identification of  
680 precipitation type at the surface, particularly when there is snow on the ground and temperatures are near 0°C,  
681 can be vital for forecasting the resulting snowpack and hydrological response. This was achieved during SAJESS  
682 by combining high temporal resolution measurements (1-minute) of precipitation amount, snow depth, and  
683 disdrometer data, with manual observations and photographic imagery of hydrometeors at the surface. Verifying  
684 the precipitation type using these measurements removes the uncertainty of precipitation type estimation that is  
685 necessary without such an array of measurements. Thirdly, observations of atmospheric conditions and  
686 precipitation aloft from the micro rain radar and upper air soundings will advance our knowledge of pre-storm  
687 conditions and the influence of tropospheric conditions on the precipitation type observed at the surface. When  
688 these conditions result in solid precipitation at the surface, inspection of the macrophotographs and MASC images  
689 can be included to confirm particle type, size, and shape, and for snow, crystal habit and riming condition. The  
690 SAJESS dataset provides an opportunity to investigate the micro-scale influences these differing particle types  
691 and crystal habits have on snowpack evolution.

692  
693 In addition, the SAJESS dataset provides the opportunity to advance forecasting and model evaluation. The  
694 breadth of instruments and human observations quantifies many parameters not archived in traditional  
695 meteorological databases. Examples of this include the non-standard timing of balloon launches, spatially  
696 distributed precipitation and temperature observations, as well as energy balance and flux data. The identification  
697 of particle type obtained by using non-standard observations such as the MASC provides ground truth to help  
698 further model microphysics.  
699

700 Finally, the SAJESS field campaign also highlights the need to enhance measurements of precipitation and snow  
701 in the upper Saint John River Basin. Near real-time access to data during the campaign allowed for the monitoring  
702 of meteorological conditions as they occurred, which can be vital for emergency management, ice jam and flood  
703 forecasting, and river navigation. This is not usually available in areas where weather or climate stations are  
704 sparse. We envision that consideration be given to furthering the meteorological monitoring network in the upper  
705 Saint John River Basin to increase the resolution and frequency of measurements and to better anticipate ice jams  
706 and major flooding events along the Saint John River.

#### 707 708 **Author contributions**

709 HDT wrote the first draft of the manuscript, as well as conducted some analyses. JMT, SJD, RES, and VV  
710 designed and led the field project. DB and LR collected manual observations during the intensive observational  
711 period. NDJ contributed to the installation of the instruments and the management of the CoCoRaHS observers.  
712 MC provided the Smart Rainfall System (SRS). HDT, JMT, SJD, RES, DB, LR, NRL, MC and VV contributed  
713 to the writing and the editing of the manuscript.

#### 714 715 **Competing interests**

716 The authors declare that they have no conflict of interest.

#### 717 718 **Data availability**

719 The SAJESS dataset (including the sample subset of data) is available from the Federated Research Data  
720 Repository (FRDR) and can be accessed at <https://doi.org/10.20383/103.0591> (Thompson et al., 2023), and is  
721 included in the Global Water Futures FRDR collection. CoCoRaHS data are available from  
722 <https://cocorahs.org/ViewData/>. SRS data are available from the Artys' web platform (<https://www1.artys.it/>) that  
723 can be accessed upon request ([m.colli@artys.it](mailto:m.colli@artys.it)). Hourly and daily data from the Edmundston ECCC station are  
724 available via the ECCC Historical data webpage, with 1-minute raw data from the station available from the  
725 authors upon request. ([https://climate.weather.gc.ca/historical\\_data/search\\_historic\\_data\\_e.html](https://climate.weather.gc.ca/historical_data/search_historic_data_e.html)).

#### 726 727 **Acknowledgments**

728 Funding was provided by the Global Water Futures programme which is project 418474-1234 funded by the  
729 Canada First Research Excellence Fund, Natural Sciences and Engineering Research Council of Canada  
730 Discovery Grants (Julie M. Thériault, Stephen J. Déry, and Ronald E. Stewart), the Canada Research Chairs

731 Program (Julie M. Thériault), and UNBC (Lisa Rickard), to conduct scientific analysis. The MUST Trailer was  
732 developed with funding from the Canadian Foundation for Innovation. Many thanks to all the volunteers and  
733 schools who collected measurements and provided locations for the SRS parabolic dishes across northwest New  
734 Brunswick during SAJESS. Thank you to Jacques Doiron, Director of the Emergency Measures for the City of  
735 Edmundston, for providing the sites, facilities and coordinating the local activity with the SAJESS team, and  
736 Amanda Ronnquist for creating the SAJESS data management plan. [We appreciate the detailed reviews and](#)  
737 [constructive comments provided by Siwei He, Robert Hellstrom, and two anonymous referees, and assistance of](#)  
738 [editor David Carlson.](#)

739

#### 740 **References**

741

742 Angulo-Martínez, M., Beguería, S., Latorre, B., and Fernández-Raga, M.: Comparison of precipitation  
743 measurements by OTT Parsivel2 and Thies LPM optical disdrometers, *Hydrological Earth System Science*, 22,  
744 2811–2837, <https://doi.org/10.5194/hess-22-2811-2018>, 2018.

745

746 Annandale, J., Jovanovic, N., Benadé, and N., Allen, R.: Software for missing data error analysis of Penman-  
747 Monteith reference evapotranspiration. *Irrigation Science*, 21, 57–67, <https://doi.org/10.1007/s002710100047>,  
748 2002.

749

750 Apogee Instruments Inc.: Infrared radiometers owner’s manual, [https://www.apogeeinstruments.com/content/SI-](https://www.apogeeinstruments.com/content/SI-400-manual.pdf)  
751 [400-manual.pdf](https://www.apogeeinstruments.com/content/SI-400-manual.pdf), last access 9 March 2023, 2023.

752

753 Beltaos, S., Ismail, S., and Burrell, B.: Midwinter breakup and jamming on the upper Saint John River: A case  
754 study, *Canadian Journal of Civil Engineering*, 30, 77-88, <https://doi.org/10.1139/102-062>, 2011.

755

756 [Budhathoki, S., Rokaya, P., & Lindenschmidt, K. E.: Impacts of future climate on the hydrology of a](#)  
757 [transboundary river basin in northeastern North America. \*Journal of Hydrology\*, 605, 127317.](#)  
758 <https://doi.org/10.1016/j.jhydrol.2021.127317>, 2022.

759

760 Buttle, J. M., Allen, D. M., Caissie, D., Davison, B., Hayashi, M., Peters, D. L., Pomeroy, J. W., Simonovic, S.,  
761 St-Hilaire, A., and Whitfield, P. H.: Flood processes in Canada: Regional and special aspects, *Canadian Water*  
762 *Resources Journal*, 41(1–2), 7–30, <https://doi.org/10.1080/07011784.2015.1131629>, 2016.  
763  
764 Campbell Scientific (2022a): IRGASON: Integrated CO2 and H2O Open-Path Gas Analyzer and 3-D Sonic  
765 Anemometer. <https://s.campbellsci.com/documents/us/manuals/irgason.pdf>, last access: 31 August 2022,  
766 20221a.  
767  
768 Campbell Scientific (2022b). EASYFLUX DL: EASYFLUX DL CR6OP or CR1KXOP For CR6 or CR1000X  
769 and Open-Path Eddy-Covariance Systems. Retrieved August 31, 2022, from  
770 <https://s.campbellsci.com/documents/us/manuals/easyflux-dl-cr6op.pdf>, last access: 6 September 2023, 2022b.  
771  
772 Cauteruccio, A., Chinchella, E., Stagnaro, M., and Lanza, L. G.: Snow particle collection efficiency and  
773 adjustment curves for the hotplate precipitation gauge. *Journal of Hydrometeorology*, 22(4), 941–954,  
774 <https://doi.org/10.1175/JHM-D-20-0149.1>, 2021.  
775  
776 Cifelli, R., Doesken, N., Kennedy, P., Carey, L. D., Rutledge, S. A., Gimmestad, C., and Depue, T.: The  
777 Community Collaborative Rain, Hail, and Snow Network: Informal education for scientists and citizens,  
778 *Bulletin of the American Meteorological Society*, 86(8), 1069–1077, <http://www.jstor.org/stable/26221344>,  
779 2005.  
780  
781 Colli, M., Cassola, F., Martina, F., Trovatore, E., Delucchi, A., Maggiolo, S., and Caviglia, D.D.: Rainfall fields  
782 monitoring based on satellite microwave down-links and traditional techniques in the city of Genoa. *IEEE*  
783 *Transactions on Geoscience Remote Sensing*, 58(9), 6266–6280, <https://doi.org/10.1109/TGRS.2020.2976137>,  
784 2020.  
785  
786 Colli, M., Stagnaro, M., Caridi, A., Lanza, L.G., Randazzo, A., Pastorino, M., Caviglia, D.D., and Delucchi, A.:  
787 A Field Assessment of a rain estimation system based on satellite-to-earth microwave links. *IEEE Transactions*  
788 *on Geoscience Remote Sensing*, 57(5), 2864–2875, <https://doi.org/10.1109/TGRS.2018.2878338>, 2019.  
789

790 Colorado Climate Center: Community collaborative rain, hail & snow network, CoCoRaHS Canada,  
791 <https://cocorahs.org/Canada.aspx>, last access 15 March 2022, 2017.  
792  
793 Domine, F., Lackner, G., Sarrazin, D., Poirier, M., and Belke-Brea, M.: Meteorological, snow and soil data  
794 (2013-2019) from a herb tundra permafrost site at Bylot Island, Canadian high Arctic, for driving and testing  
795 snow and land surface models, *Earth System Science Data*, 13(9), 4331–4348. [https://doi.org/10.5194/essd-13-](https://doi.org/10.5194/essd-13-4331-2021)  
796 4331-2021, 2021.  
797  
798 Environment and Climate Change Canada: Top ten weather stories for 2008: story four: Saint John River floods  
799 from top to bottom, <https://www.ec.gc.ca/meteo-weather/default.asp?lang=En&n=7D6FDB7C-1>, last access 25  
800 March 2023, 2017.  
801  
802 Environment and Climate Change Canada: Canada's top 10 weather stories of 2018: 7. Flash flooding of the  
803 Saint John River, [https://www.canada.ca/en/environment-climate-change/services/top-ten-weather-](https://www.canada.ca/en/environment-climate-change/services/top-ten-weather-stories/2018.html#toc6)  
804 stories/2018.html#toc6, last access 25 March 2023, 2019.  
805  
806 Environment and Climate Change Canada: Canada's top 10 weather stories of 2019: 9. Saint John River floods  
807 again. [https://www.canada.ca/en/environment-climate-change/services/top-ten-weather-](https://www.canada.ca/en/environment-climate-change/services/top-ten-weather-stories/2019.html#toc10)  
808 stories/2019.html#toc10, last access 25 March 2023, 2020.  
809  
810 Falconi, M.T., von Lerber, A., Ori, D., Silvio Marzano, F., and Moisseev, D.: Snowfall retrieval at X, Ka and W  
811 bands: consistency of backscattering and microphysical properties using BAECC ground-based measurements,  
812 *Atmospheric Measurement Techniques*, 11, 3059-3079, <https://doi.org/10.5194/amt-11-3059-2018>, 2018.  
813  
814 Fitch, K. E., Hang, C., Talaei, A., and Garrett, T. J.: Arctic observations and numerical simulations of surface  
815 wind effects on Multi-Angle Snowflake Camera measurement, *Atmospheric Measurement Techniques*, 14(2),  
816 1127–1142. <https://doi.org/10.5194/amt-14-1127-2021>, 2021.  
817  
818 Foken, T., Gööckede, M., Mauder, M., Mahrt, L., Amiro, B., and Munger, W.: Post-Field Data Quality Control.  
819 In: Lee, X., Massman, W., Law, B. (eds) *Handbook of Micrometeorology*, Atmospheric and Oceanographic  
820 Sciences Library, vol 29, Springer, Dordrecht, [https://doi.org/10.1007/1-4020-2265-4\\_9](https://doi.org/10.1007/1-4020-2265-4_9), 2004.

821  
822 Fortin, G., and Dubreuil, V.: A geostatistical approach to create a new climate types map at regional scale: case  
823 study of New Brunswick, Canada. *Theoretical and Applied Climatology*, 139(1–2), 323–334,  
824 <https://doi.org/10.1007/s00704-019-02961-2>, 2020.  
825  
826 Garrett, T. J., Fallgatter, C., Shkurko, K., and Howlett, D.: Fall speed measurement and high-resolution multi-  
827 angle photography of hydrometeors in free fall, *Atmospheric Measurement Techniques*, 5, 2625–2633,  
828 <https://doi.org/10.5194/amt-5-2625-2012>, 2012.  
829  
830 Giannetti, F., and Reggiani, R.: Opportunistic rain rate estimation from measurements of satellite downlink  
831 attenuation: A survey. *Sensors*, 21(17), 5872, <https://doi.org/10.3390/s21175872>, 2021.  
832  
833 Gibson, S. R., and Stewart, R. E.: Observations of ice pellets during a winter storm. *Atmospheric Research*,  
834 85(1), 64–76. <https://doi.org/10.1016/j.atmosres.2006.11.004>, 2007  
835  
836 Hicks, A., and Notaroš, B. M.: Method for classification of snowflakes based on images by a multi-angle  
837 snowflake camera using convolutional neural networks. *Journal of Atmospheric and Oceanic Technology*,  
838 36(12), 2267–2282, <https://doi.org/10.1175/JTECH-D-19-0055.1>, 2019.  
839  
840 [Houze, R. A., McMurdie, L. A., Petersen, W. A., Schwall Er, M. R., Baccus, W., Lundquist, J. D., Mass, C. F.,](#)  
841 [Nijssen, B., Rutledge, S. A., Hudak, D. R., Tanelli, S., Mace, G. G., Poellot, M. R., Lettenmaier, D. P.,](#)  
842 [Zagrodnik, J. P., Rowe, A. K., DeHart, J. C., Madaus, L. E., & Barnes, H. C.: The olympic mountains](#)  
843 [experiment \(Olympex\). \*Bulletin of the American Meteorological Society\*, 98\(10\), 2167–2188,](#)  
844 <https://doi.org/10.1175/BAMS-D-16-0182.1>, 2017.  
845  
846 [Ishizaka, M., Motoyoshi, H., Nakai, S., Shiina, T., Kumakura, T., & Muramoto, K. I.: A new method for](#)  
847 [identifying the main type of solid hydrometeors contributing to snowfall from measured size-fall speed](#)  
848 [relationship. \*Journal of the Meteorological Society of Japan\*, 91\(6\), 747–762. <https://doi.org/10.2151/jmsj.2013->](#)  
849 [602, 2013.](#)  
850



851 Joe, P., Scott, B., Doyle, C., Isaac, G., Gulpepe, I., Forsyth, D., Cober, S., Campos, E., Heckman, I., Donaldson,  
852 N., Hudak, D., Rasmussen, R., Kucera, P., Stewart, R., Thériault, J. M., Fisco, T., Rasmussen, K. L.,  
853 Carmichael, H., Laplante, A., ... and Boudala, F.: The Monitoring network of the Vancouver 2010 Olympics,  
854 Pure and Applied Geophysics, 171(1–2), 25–58, <https://doi.org/10.1007/s00024-012-0588-z>, 2014.  
855  
856 Kenny, J. L., and Secord, A. G.: Engineering modernity: Hydroelectric development in New Brunswick, 1945-  
857 1970, *Acadiensis*, 39(1), 3–26, 2010.  
858  
859 Kochendorfer, J., Rasmussen, R., Wolff, M., Baker, B., Hall, M. E., Meyers, T., Landolt, S., Jacheik, A.,  
860 Isaksen, K., Brækkan, R., and Leeper, R.: The quantification and correction of wind-induced precipitation  
861 measurement errors. *Hydrology and Earth System Sciences*, 21(4), 1973–1989, [https://doi.org/10.5194/hess-21-](https://doi.org/10.5194/hess-21-1973-2017)  
862 [1973-2017](https://doi.org/10.5194/hess-21-1973-2017), 2017.  
863  
864 Liao, L., Meneghini, R., Tokay, A., and Bliven, L. F.: Retrieval of snow properties for Ku- and Ka-band dual-  
865 frequency radar, *Journal of Applied Meteorology and Climatology*, 55(9), 1845-1858,  
866 <https://doi.org/10.1175/JAMC-D-15-0355.1>, 2016.  
867  
868 Lapo, K. E., Hinkelman, L. M., Landry, C. C., Massmann, A. K., and Lundquist, J. D.: A simple algorithm for  
869 identifying periods of snow accumulation on a radiometer, *Water Resources Research*, 51, 7820– 7828,  
870 [doi:10.1002/2015WR017590](https://doi.org/10.1002/2015WR017590), 2015.  
871  
872 Maahn, M., and Kollias, P.: Improved Micro Rain Radar snow measurements using Doppler spectra post-  
873 processing. *Atmospheric Measurement Techniques*, 5(11), 2661–2673. [https://doi.org/10.5194/amt-5-2661-](https://doi.org/10.5194/amt-5-2661-2012)  
874 [2012](https://doi.org/10.5194/amt-5-2661-2012), 2012.  
875  
876 [Marwitz, J.: A comparison of winter orographic storms over the San Juan Mountains and the Sierra Nevada.](#)  
877 [Precipitation Enhancement—A Scientific Challenge, Meteorological Monographs., No. 21, Amer. Meteor. Soc.,](#)  
878 [109–113, \[https:// doi.org/10.1175/0065-9401-21.43.109\]\(https://doi.org/10.1175/0065-9401-21.43.109\), 1986.](#)  
879

880 METEK: MRR Physical Basics, 5.2.0.1,  
881 [https://mpimet.mpg.de/fileadmin/atmosphaere/barbados/Instrumentation/MRR-physical-basics\\_20090707.pdf](https://mpimet.mpg.de/fileadmin/atmosphaere/barbados/Instrumentation/MRR-physical-basics_20090707.pdf),  
882 last access: 25 March 2023, 2009.  
883  
884 METEK: Micro Rain Radar MRR-2, [https://metek.de/wp-content/uploads/2014/05/Datasheet\\_MRR-2.pdf](https://metek.de/wp-content/uploads/2014/05/Datasheet_MRR-2.pdf), last  
885 access 22 June 2022, 2010.  
886  
887 METEK: Micro Rain Radar MRR-PRO, [https://metek.de/wp-](https://metek.de/wp-content/uploads/2016/12/20180206_Datenblatt_MRR-PRO.pdf)  
888 [content/uploads/2016/12/20180206\\_Datenblatt\\_MRR-PRO.pdf](https://metek.de/wp-content/uploads/2016/12/20180206_Datenblatt_MRR-PRO.pdf), last access 22 June 2022, 2017.  
889  
890 [Minder, J. R., Bassill, N., Fabry, F., French, J. R., Friedrich, K., Gultepe, I., Gyakum, J., Kingsmill, D. E.,](#)  
891 [Kosiba, K., Lachapelle, M., Michelson, D., Nichman, L., Nguyen, C., Thériault, J. M., Winters, A. C., Wolde,](#)  
892 [M., & Wurman, J.: P-Type Processes and Predictability: The Winter Precipitation Type Research Multiscale](#)  
893 [Experiment \(WINTRE-MIX\). \*Bulletin of the American Meteorological Society\*, 104\(8\), E1469-E1492.](#)  
894 <https://doi.org/10.1175/BAMS-D-22-0095.1>, 2023.  
895  
896 Newton, B., and Burrell, B. C.: The April–May 2008 flood event in the Saint John River Basin: Causes,  
897 assessment, and damages. *Canadian Water Resources Journal*, 41(1–2), 118–128.  
898 <https://doi.org/10.1080/07011784.2015.1009950>, 2016.  
899  
900 Nitu, R., Roulet, Y., Wolff, M., Earle, M., Reverdin, A., Smith, C., Kochendorfer, J., Morin, S., Rasmussen, R.,  
901 Wong, K., Alastrué, J., Arnold, L., Baker, B., Buisan, S., Collado, J. L., Colli, M., Collins, B., Gaydos, A.,  
902 Hannula, H.-R., . . . , and Senese, A.: WMO Solid Precipitation Intercomparison Experiment (SPICE) (2012-  
903 2015), 131, World Meteorological Organization, 1429 pp.,  
904 [https://library.wmo.int/doc\\_num.php?explnum\\_id=5686](https://library.wmo.int/doc_num.php?explnum_id=5686), 2018.  
905  
906 Onset Computer Corporation: Hobo temperature/RH data logger, HOBO Temperature/RH Data Logger  
907 MX2301A | Onset Data Loggers, <https://www.onsetcomp.com/products/data-loggers/mx2301a/>, last access 15  
908 March 2022, 2022.  
909

910 [OTT: Operating instructions Present Weather Sensor OTT Parsivel<sup>2</sup>](https://www.ott.com/download/operating-instructions-present-weather-sensor-ott-parsivel2-with-screen-heating-2/). [https://www.ott.com/download/operating-](https://www.ott.com/download/operating-instructions-present-weather-sensor-ott-parsivel2-with-screen-heating-2/)  
911 [instructions-present-weather-sensor-ott-parsivel2-with-screen-heating-2/](https://www.ott.com/download/operating-instructions-present-weather-sensor-ott-parsivel2-with-screen-heating-2/). Last access 5 September 2023, 2019.  
912  
913 Pond Engineering: K63 Hotplate total precipitation gauge, <http://www.pondengineering.com/k63>, last access 25  
914 March 2023, 2021.  
915  
916 Praz, C., Roulet, Y. A., and Berne, A.: Solid hydrometeor classification and riming degree estimation from  
917 pictures collected with a Multi-Angle Snowflake Camera. *Atmospheric Measurement Techniques*, 10(4), 1335–  
918 1357, <https://doi.org/10.5194/amt-10-1335-2017>, 2017.  
919  
920 [Rasmussen, R. M., Vivekanandan, J., Cole, J., Myers, B., & Masters, C.: The estimation of snowfall rate using](https://doi.org/10.1175/1520-0450(1999)038<1542:TEOSRU>2.0.CO;2)  
921 [visibility](https://doi.org/10.1175/1520-0450(1999)038<1542:TEOSRU>2.0.CO;2). *Journal of Applied Meteorology*, 38(10), 1542–1563. [https://doi.org/10.1175/1520-](https://doi.org/10.1175/1520-0450(1999)038<1542:TEOSRU>2.0.CO;2)  
922 [0450\(1999\)038<1542:TEOSRU>2.0.CO;2](https://doi.org/10.1175/1520-0450(1999)038<1542:TEOSRU>2.0.CO;2), 1999.  
923  
924 Rasmussen, R. M., Hallett, J., Purcell, R., Landolt, S. D., and Cole, J.: The hotplate precipitation gauge, *Journal*  
925 *of Atmospheric and Oceanic Technology*, 28(2), 148–164, <https://doi.org/10.1175/2010JTECHA1375.1>, 2011.  
926  
927 Raupach, T. H., and Berne, A.: Correction of raindrop size distributions measured by Parsivel disdrometers,  
928 using a two-dimensional video disdrometer as a reference, *Atmospheric Measurement Techniques*, 8(1), 343–  
929 365. <https://doi.org/10.5194/amt-8-343-2015>, 2015.  
930  
931 Schaer, M., Praz, C., and Berne, A.: Identification of blowing snow particles in images from a Multi-Angle  
932 Snowflake Camera. *Cryosphere*, 14(1), 367–384, <https://doi.org/10.5194/tc-14-367-2020>, 2020.  
933  
934 Sicart, J.E., Pomeroy, J.W., Essery, R.L.H. and Bewley, D.: Incoming longwave radiation to melting snow:  
935 observations, sensitivity and estimation in Northern environments, *Hydrological Processes*, 20, 3697-3708,  
936 <https://doi.org/10.1002/hyp.6383>, 2006.  
937  
938 Skofronick-Jackson, G., Hudak, D., Petersen, W., Nesbitt, S. W., Chandrasekar, V., Durden, S., Gleicher, K. J.,  
939 Huang, G. J., Joe, P., Kollias, P., Reed, K. A., Schwaller, M. R., Stewart, R., Tanelli, S., Tokay, A., Wang, J. R.,  
940 and Wolde, M.: Global precipitation measurement cold season precipitation experiment (GCPEX): For

941 measurement's sake, let it snow. *Bulletin of the American Meteorological Society*, 96(10), 1719–1741,  
942 <https://doi.org/10.1175/BAMS-D-13-00262.1>, 2015.

943

944 Souverijns, N., Gossart, A., Lhermitte, S., Gorodetskaya, I. V., Kneifel, S., Maahn, M., Bliven, F. L., & van  
945 Lipzig, N. P. M.: Estimating radar reflectivity - Snowfall rate relationships and their uncertainties over  
946 Antarctica by combining disdrometer and radar observations. *Atmospheric Research*, 196(June), 211–223.  
947 <https://doi.org/10.1016/j.atmosres.2017.06.001>, 2017.

948

949 [Stewart, R. E., Shaw, R. W., & Isaac, G. A.: Canadian Atlantic Storms Program: The meteorological field](http://www.jstor.org/stable/26225054)  
950 [project. \*Bulletin of the American Meteorological Society\*, 68\(4\), 338–345.](http://www.jstor.org/stable/26225054)  
951 <http://www.jstor.org/stable/26225054>, 1987.

952

953 Stewart, R. E.: Canadian Atlantic Storms Program: Progress and plans of the meteorological component.  
954 *Bulletin of the American Meteorological Society*, 72(3), 364–371. [https://doi.org/10.1175/1520-](https://doi.org/10.1175/1520-0477(1991)072<0364:CASPPA>2.0.CO;2)  
955 [0477\(1991\)072<0364:CASPPA>2.0.CO;2](https://doi.org/10.1175/1520-0477(1991)072<0364:CASPPA>2.0.CO;2), 1991

956

957 Thériault, J. M., Hung, I., Vaquer, P., Stewart, R. E., and Pomeroy, J.: Precipitation characteristics and  
958 associated weather conditions on the eastern slopes of the Rocky Mountains during March and April 2015I,  
959 *Hydrology and Earth System Sciences*, 22(8), 4491–4512, <https://doi.org/10.5194/hess-22-4491-2018>, 2018.

960

961 Thériault, J. M., Déry, S. J., Pomeroy, J. W., Smith, H. M., Almonte, J., Bertonecini, A., Crawford, R. W.,  
962 Desroches-Lapointe, A., Lachapelle, M., Mariani, Z., Mitchell, S., Morris, J. E., Hébert-Pinard, C., Rodriguez,  
963 P., and Thompson, H. D.: Meteorological observations collected during the Storms and Precipitation across the  
964 continental Divide Experiment (SPADE), April-June 2019, *Earth System Science Data*, 13(3), 1233–1249,  
965 <https://doi.org/10.5194/essd-13-1233-2021>, 2021a.

966

967 Thériault, J. M., Leroux, N. R., and Rasmussen, R. M.: Improvement of solid precipitation measurements using  
968 a hotplate precipitation gauge, *Journal of Hydrometeorology*, 22(4), 877–885, [https://doi.org/10.1175/JHM-D-](https://doi.org/10.1175/JHM-D-20-0168.1)  
969 [20-0168.1](https://doi.org/10.1175/JHM-D-20-0168.1), 2021b.

970

971 [Thériault, J. M., Leroux, N. R., Stewart, R. E., Bertoncini, A., Déry, S. J., Pomeroy, J. W., Thompson, H. D.,](#)  
972 [Smith, H., Mariani, Z., Desroches-Lapointe, A., Mitchell, S., & Almonte, J.:](#) Storms and Precipitation across the  
973 [continental Divide Experiment \(SPADE\). Bulletin of the American Meteorological Society, 103\(11\), E2628–](#)  
974 [E2649. <https://doi.org/10.1175/BAMS-D-21-0146.1>. 2022.](#)  
975  
976 Thompson, H. D., Thériault, J. M., Déry, S. J., Stewart, R. E., Boisvert, D., Rickard, L., Leroux, N. R., Colli,  
977 M., and Vincent Vionnet, V.: Atmospheric and surface observation data collected during the Saint John River  
978 Experiment on Cold Season Storms, Federated Research Data Repository [data set],  
979 <https://doi.org/10.20383/103.059>, 2023.  
980  
981 Tokay, A., Hartmann, P., Battaglia, A., Gage, K. S., Clark, W. L., and Williams, C. R.: A field study of  
982 reflectivity and Z-R relations using vertically pointing radars and disdrometers, *Journal of Atmospheric and*  
983 *Oceanic Technology*, 26(6), 1120–1134, <https://doi.org/10.1175/2008JTECHA1163.1>, 2009.  
984  
985 US Department of Energy: Toolbox — A rolling list of software/packages for flux-related data processing,  
986 FLUXNET: The Data Portal Serving the FLUXNET Community, [https://fluxnet.org/2017/10/10/toolbox-a-](https://fluxnet.org/2017/10/10/toolbox-a-rolling-list-of-softwarepackages-for-flux-related-data-processing/)  
987 [rolling-list-of-softwarepackages-for-flux-related-data-processing/](https://fluxnet.org/2017/10/10/toolbox-a-rolling-list-of-softwarepackages-for-flux-related-data-processing/), last access 31 August 2022, 2021.

988 **Table 1. Primary site information**

Location	Lat (°N)	Lon (°W)	Elevation (m)	Surface	Surroundings	Dates of operation for SAJESS
Fixed Station	47.418	68.324	152	Grassland on gravel riverbed	Open grassland in broad river valley, rural road ~150 m to the west	1 December 2020 – 30 April 2021
MUST Trailer	47.361	68.320	143	Packed gravel, short grass	Site on edge of city treatment ponds, ~ 250 m from confluence of two large rivers; suburban subdivision to the north,	1 March 2021 – 30 April 2021

989  
990  
991

992 **Table 2. Instrument details for the SAJESS Fixed Station site**

Installation (instrument abbr.)	Instrument	Installation height	Variable	Units	Resolution	Accuracy
Met tripod (MET)	Campbell Scientific CR1000X datalogger	1.5 m	data recording	NA	NA	NA
	OTT Parsivel <sup>2</sup> disdrometer	2.80 m	Timestamp Intensity of precipitation (mm/h) Precipitation since start (mm) Weather code SYNOP WaWa Weather code METAR/SPECI Weather code NWS Radar reflectivity (dBz) MOR Visibility (m) Signal amplitude of Laserband Number of detected particles Temperature in sensor (°C) Heating current (A) Sensor voltage (V) Kinetic Energy Snow intensity (mm/h) V0D0 ... V31D31	Timestamp mm h <sup>-1</sup> Mm val val val dBz m val val °C A V J (m <sup>2</sup> h) <sup>-1</sup> mm h <sup>-1</sup> val	1 min (average), except for the VxDx size and fallspeed classes, which represent a 1 min sum	Accuracy is not given by OTT for the individual variables, however the size classification are not given by OTT±1 size class (0.2 to 2 mm) ±0.5 size class (>2mm)
	Vaisala HMP155 temperature /RH probe	2.00 m	Air temperature Relative Humidity	°C %	1 min (average)	0.226+0.0028×reading (-80 to +20 °C) 0.055+0.0057×reading (+20 to +60 °C)
	Kipp & Zonen CNR4	1.80 m	4-way net radiation	W m <sup>-2</sup>	1 min (average)	< 5 %

	Net radiometer					
	Campbell Scientific SR50A sonic ranger	1.80 m	Snow depth	m	1 min (average)	±1 cm
	Apogee SI-411 IR radiometer	1.80 m	Surface temperature	°C	1 min (average)	±0.2 °C
	Campbell Scientific CS655 Soil probe (vertically)	0.00 m	Soil temperature Soil moisture content Soil electrical conductivity	°C % dS m <sup>-1</sup>	1 min (average)	±0.1 - 0.5 °C ±1 - 3% ±5% of reading + 0.05 dS m <sup>-1</sup>
MRR tripod (MRR)	METEK MRR-2	2.60 m	Doppler raw spectra Reflectivity (Ze) Doppler velocity (W) Spectral width (σ)	dB dBz m s <sup>-1</sup> m s <sup>-1</sup>	10 sec raw data; 1 min average; see Section 3.1.5	0.53 dB 0.53 dBZ 0.109 ms <sup>-1</sup> 0.09 ms <sup>-1</sup>
Hotplate tripod (HP)	Pond engineering K63 Hotplate precipitation gauge	2.60 m	Air temperature Barometric pressure Precipitation rate Accumulation Windspeed Hotplate power	°C kPa mm hr <sup>-1</sup> mm m s <sup>-1</sup> W	1 min (average) 5 min (average)	±1 °C ±1 kPa ±0.5 mm hr <sup>-1</sup> ±0.5 mm ±1 ms <sup>-1</sup> NA
Flux tripod (FLUX)	Campbell Scientific CR1000X datalogger	1.5 m	data recording	NA	NA	NA
	Vaisala HMP155 Temperature /RH probe	2.00 m	Air temperature Relative humidity	°C %	30 min (average)	0.226+0.0028×reading (-80 to +20 °C) 0.055+0.0057×reading (+20 to +60 °C)



	Apogee SI-411 Infrared radiometer	1.80 m	Surface temperature	°C	30 min (average)	±0.2 °C
	Kipp & Zonen CNR4 Net radiometer	1.80 m	4-way net radiation	W m <sup>-2</sup>	30 min (average)	< 5 %
	Campbell Scientific IRGASON	2.00 m	3D wind CO2 density H2O density Sonic temperature	m s <sup>-1</sup> mg·m <sup>-3</sup> g·m <sup>-3</sup> °C	10 Hz	1 mm s <sup>-1</sup> 0.2 mg·m <sup>-3</sup> (0.15 µmol·mol <sup>-1</sup> ) 0.00350 g·m <sup>-3</sup> (0.006 mmol·mol <sup>-1</sup> ) 0.025 °C
	Campbell Scientific CS655 Soil probe	2.5 cm below surface	Soil temperature Soil moisture content Soil electrical conductivity	°C % dS m <sup>-1</sup>	30 min (average)	±0.1 - 0.5 °C ±1 - 3% ±5% of reading + 0.05 dS m <sup>-1</sup>
	Campbell Scientific HFP01 Soil heat flux plates	8 cm below surface	Soil heat flux	W m <sup>-2</sup>	30 min (average)	-15% to +5% in most common soils

993  
994  
995  
996

Table 3. Instrument details for the SAJESS MUST Trailer site

Installation (Instrument abbr.)	Instrument	Installation height	Variable	Units	Resolution	Accuracy
Met tripod (MET)	Campbell Scientific CR1000X datalogger	1.5 m	data recording	NA	NA	NA
	Vaisala HMP155 Temperature/RH probe	2.00 m	Air temperature Relative humidity	°C %	1 min (average)	$0.226+0.0028 \times \text{reading}$ (-80 to +20 °C) $0.055+0.0057 \times \text{reading}$ (+20 to +60 °C)
	Kipp & Zonen CNR4 Net radiometer	1.80 m	Net 4-way radiation	W m <sup>-2</sup>	1 min (average)	< 5 %
	Campbell Scientific SR50A	1.80 m	Snow depth	m	1 min (average)	±1 cm
10 m Mast (MAST)	Campbell Scientific CR1000X datalogger	1.5 m	data recording	NA	NA	NA
	Pond engineering K63 Hotplate precipitation gauge	2.60 m	Air temperature Barometric pressure Precipitation rate Accumulation Windspeed Hotplate power	°C kPa mm hr <sup>-1</sup> mm m s <sup>-1</sup> W	1 min (average) 5 min (average)	±1 °C ±1 kPa ±0.5 mm hr <sup>-1</sup> ±0.5 mm ±1 ms <sup>-1</sup> NA
MASC Platform (MASC)	Multi-angle snowflake camera	1.00 m	Series of 3 images	NA	Up to 3 Hz	NA
MRR Pro (MRR)	METEK MRR Pro	1.30 m	Doppler raw spectra Reflectivity (Ze) Doppler velocity (W) Spectral width (σ)	dB dBz m s <sup>-1</sup> m s <sup>-1</sup>	see Section 3.1.5	0.53 dB 0.53 dBZ 0.109 ms <sup>-1</sup> 0.09 ms <sup>-1</sup>
Macrophotography (MP)	Nikon D80 with 60 mm macro lens	NA	Series of 9 images	N/A	10 min	NA

Manual observations (OBS)	Volunteer and/or student	NA	Sky condition Cloud type Precipitation type Blowing snow Light precipitation	Oktas Type Type Y/N Y/N	10 min	NA
Upper air observations (SB)	iMet-3050A 403 MHz portable sounding system with iMet-4 radiosonde	NA	Air temperature Relative humidity Wind speed Wind direction Pressure Geopotential height	°C % m s <sup>-1</sup> degree s hPa m	1 sec	± 0.5 - 1.0 °C ± 5% ± 0.5 m s <sup>-1</sup> ± 1 degrees ± 0.5 - 2.0 hPa ± 15 m

998

999  
1000  
1001  
1002

**Table 4. Locations of CoCoRaHS stations founded during SAJESS, with HOBO MX2301A Temperature/RH information (if present)**

CoCoRaHS ID	Temp/RH sensor ID (if present)	Lat (°N)	Lon (°W)	Elevation (m)	Temp/RH sensor period of record
CAN-NB-111	SJ_HOBOTEMP_01	47.37	68.32	166	11/12/2020 – 30/04/2021
CAN-NB-112	Not present	47.35	68.67	198	
CAN-NB-113	SJ_HOBOTEMP_02	47.25	68.03	155	11/12/2020 – 30/04/2021
CAN-NB-114	SJ_HOBOTEMP_03	47.37	68.31	197	10/12/2020 – 30/04/2021
CAN-NB-115	SJ_HOBOTEMP_04	47.43	68.39	142	10/12/2020 – 30/04/2021
CAN-NB-117	SJ_HOBOTEMP_05	47.45	68.32	326	11/12/2020 – 30/04/2021
CAN-NB-121	Not present	47.21	67.96	154	
CAN-NB-122	Not present	47.40	68.34	144	
CAN-NB-126	Not present	47.38	68.31	192	
CAN-NB-127	SJ_HOBOTEMP_06	47.36	68.16	176	05/03/2021 – 30/04/2021
CAN-NB-133	SJ_HOBOTEMP_07	47.35	68.46	332	05/03/2021 – 30/04/2021
CAN-NB-134	Not present	47.28	68.41	155	
CAN-NB-135	SJ_HOBOTEMP_08	47.26	68.61	167	12/12/2020 – 30/04/2021
CAN-NB-139	SJ_HOBOTEMP_09	47.37	68.34	241	10/12/2020 – 30/04/2021
CAN-NB-140	Not present	47.36	67.97	295	
CAN-NB-141	Not present	47.43	68.29	348	
CAN-NB-142	Not present	47.36	68.36	189	
CAN-NB-143	SJ_HOBOTEMP_10	47.24	68.70	170	12/12/2020 – 30/04/2021
CAN-NB-144	SJ_HOBOTEMP_11	47.37	68.28	141	10/12/2020 – 30/04/2021
CAN-NB-145	SJ_HOBOTEMP_12	47.33	68.09	231	05/03/2020 – 30/04/2021
CAN-NB-147	Not present	47.35	68.22	164	
N/A	SJ_HOBOTEMP_13	47.29	68.39	156	05/03/2021 – 30/04/2021

1003